Agricultural Water Management 322 (2025) 109984

Contents lists available at ScienceDirect

Agricultural Water Management

journal homepage: www.elsevier.com/locate/agwat

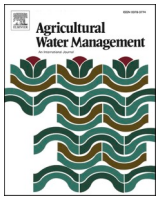

Energy flux, evapotranspiration, and crop coefficients of drip-irrigated kiwifruit and citrus orchards in Southwest China

Ningbo Cui [a], Chenggaoge Yang [a], Xiuyun Yu [a], Daozhi Gong [b], Yu Feng [c], Xiaoxian Zhang [d], Lu Zhao [a], Zhihui Wang [a], Jingyuan Xue [e], Shouzheng Jiang [a,*]

[a] State Key Laboratory of Hydraulics and Mountain River Engineering & College of Water Resource and Hydropower, Sichuan University, Chengdu 610065, China
[b] State Engineering Laboratory of Efficient Water Use of Crops and Disaster Loss Mitigation, Institute of Environment and Sustainable Development in Agriculture, Chinese Academy of Agriculture Science, Beijing 100081, China
[c] Ningbo Institute of Digital Twin, Eastern Institute of Technology, Ningbo 315200, China
[d] Department of Sustainable Soils and Grassland Systems, Rothamsted Research, Harpenden, Hertfordshire AL5 2JQ, United Kingdom
[e] Institute for Disaster Management and Reconstruction, Sichuan University, Chengdu 610041, China

ARTICLE INFO

Handling Editor - Dr X Zhang

Keywords:
Crop water use
Perennial orchard
Vegetation cover
Evapotranspiration
Energy partitioning

ABSTRACT

Studying crop water use and developing reliable estimation methods are essential for evapotranspiration (*ET*) estimation and irrigation schedule formulation. Eddy covariance system observations were conducted to investigate the seasonal variations of energy flux, evapotranspiration (*ET*), crop coefficients (K_c) and basal K_c (K_{cb}) in drip-irrigated kiwifruit (3 years) and citrus (4 years) widely planted in Southwest China. Energy partitioning showed significant seasonal and diurnal variations during the growing seasons, and most net radiation was consumed by latent heat flux, with ratios of 70.9 % in kiwifruit and 69.9 % in citrus orchard, respectively. The average *ET* and *T* were estimated at 2.04 ± 0.18 mm d^{-1} and 1.15 ± 0.16 mm d^{-1} for kiwifruit, and 2.49 ± 0.25 mm d^{-1} and 1.18 ± 0.09 mm d^{-1} for citrus orchard, respectively. The derived transferable, standard K_c ($K_{c\text{-standard}}$) for kiwifruit was 0.74 ± 0.01 at the initial stage ($K_{c\text{-ini}}$), 0.99 ± 0.02 at the mid-season stage ($K_{c\text{-mid}}$), and 0.82 ± 0.01 at the late-season stage ($K_{c\text{-end}}$), while the stagewise value for $K_{cb\text{-standard}}$ was 0.24 ± 0.09 ($K_{cb\text{-ini}}$), 0.58 ± 0.05 ($K_{cb\text{-mid}}$) and 0.63 ± 0.09 ($K_{cb\text{-end}}$). The derived $K_{c\text{-standard}}$ values were 0.92 ±0.03, 1.01 ±0.03, and 0.95 ±0.07 at the citrus initial, mid-season, and late-season stages, while the standard citrus $K_{cb\text{-ini}}$, $K_{cb\text{-mid}}$ and $K_{cb\text{-end}}$ were derived at 0.59 ±0.03, 0.61 ±0.02 and 0.69 ±0.03, respectively. The locally developed daily K_c and K_{cb} were effectively regulated by leaf area index, growing degree days and underlying conductance in both perennial cash orchards. Seasonal rainfall and vegetation cover greatly affected orchard locally K_c due to the changes in soil surface moisture and coverage, especially in citrus orchards planted with wide rows. The calibrated K_c and K_{cb} can serve as valuable guidelines for assessing the actual *ET* and precise irrigation water management of extensively planted kiwifruit and citrus orchards in Southwest China.

1. Introduction

Evapotranspiration (*ET*) plays a vital role in sustaining water and energy balance in agricultural ecosystems, particularly in areas with limited water resources and arid or semi-arid areas. In-depth studies on cropland *ET* are vital for managing water resources, optimizing irrigation schedules, improving water use efficiency, and advancing agro-ecosystem hydrologic process research (Cui et al., 2023; Segovia-Cardozo et al., 2022). *ET* generally comprises transpiration (*T*) and evaporation (*E*, including soil evaporation (E_s) and canopy-intercepted evaporation (E_i)). *T* denotes the transfer of water from the soil to the atmosphere via crop organs or tissues, intimately associated with crop physiological activities like photosynthesis, stomatal behavior, and nutrient transport processes (Jiang et al., 2019b; Kool et al., 2018). *E* refers to the unproductive loss of water through the soil or the wet crop canopy, which is essential for creating suitable environmental conditions for crop development (Kool et al., 2018). Accurate quantification of crop *ET* and water use is the premise for determining irrigation timing and water volume, serving as a foundation for eco-hydrological studies and irrigation water management (Pereira et al., 2021a).

Various techniques have been established to assess *ET* and its

* Corresponding author.
E-mail address: jiangshouzheng@scu.edu.cn (S. Jiang).

https://doi.org/10.1016/j.agwat.2025.109984
Received 12 July 2025; Received in revised form 10 November 2025; Accepted 10 November 2025
Available online 27 November 2025

components, including sap flow and micro-lysimeters (Mly) (Mobe et al., 2020; Peddinti and Kambhammettu, 2019), and large weighing lysimeters (Bian et al., 2024; Segovia-Cardozo et al., 2022). The issue of upscaling canopy transpiration and sap flow calculations remains controversial (Wiedemann et al., 2016; Flo et al., 2019), and there are great uncertainties in *ET* and *E* measurements obtained from lysimeters because of their limited representative areas (Wang et al., 2020; Gong et al., 2020). The EC and large-aperture scintillometers with a Bowen ratio system (Anapalli et al., 2020; Zhao et al., 2021) offer direct and precise methods for measuring *ET* over short intervals, such as 30 min, without disturbing the underlying surface (e.g., 30 min); its representative area is much larger compared to that of a lysimeter (Guo et al., 2020). However, long-term continuous observation and maintenance for such equipment are challenging and expensive. Consequently, estimating crop *ET* using models is more straightforward and significant in practical applications. Various models estimate *ET* from hydrological or micrometeorological perspectives, such as the multisource Priestley-Taylor model (P-T model, T plus E_{Soil} plus E_i) (Gan and Liu, 2020), thermal-based surface energy balance models (Burchard-Levine et al., 2022; Mebrie et al., 2023), and Penman-Monteith (PM) models, which assume heat and water vapor occur at the same level (Ershadi et al., 2015). The PM model is extensively used owing to its robust physical mechanisms for depicting the water and heat transport processes. In addition, it serves as a theoretical basis for other variations in P-M-type models (Ershadi et al., 2015). For example, the Shuttleworth–Wallace models partition the evaporative source into distinct patches and compute the individual *ET* components by formulating separate energy balance equations for each patch (Cui et al., 2023; Jiang et al., 2019b). However, the practical use of P-M-type models is hindered by uncertainties, particularly due to the extensive and contentious measurements required for variables like minimum stomatal resistance (Ershadi et al., 2015; Jiang et al., 2022a).

The most prevalent and effective method to estimate crop *ET* is the crop coefficient method, as identified by Allen et al. (1998), crop *ET* can be determined by integrating crop characteristics (e.g., crop coefficient [K_c]), weather parameters (i.e., reference evapotranspiration [ET_o]), and management practices (e.g., treatments imposed) (Gong et al., 2017, 2019). The K_c is primarily influenced by specific crop features rather than by climate, enabling an easy adaptation of standard K_c values to region-specific values based on location and climate (Petry et al., 2024; Wang et al., 2023). Two distinct crop *ET* approaches are outlined in the FAO-56 document: the single-crop coefficient method and the dual-crop coefficient method. The single-crop coefficient approach is used to quantify total water use and is primarily used for irrigation management because of its simplicity and scalability (Pereira et al., 2021b; Zhao et al., 2021). The dual-crop coefficient approach is extensively employed to assess *E* and *T* based on two separate coefficients (i.e., basal crop coefficient [K_{cb}] and soil evaporation coefficient [K_e]) (Gong et al., 2019; Mobe et al., 2020; Segovia-Cardozo et al., 2022). Several studies indicate that the dual-crop coefficient technique surpasses alternatives in estimating *ET*, underscoring its significance in evaluating water-saving strategies and sustainable water management (Anderson et al., 2017). Although FAO-56 provides a relatively substantial method for crop water requirement estimation, many studies have shown that site-specific K_c and K_{cb} may deviate from FAO-56 tabulated values as they change across locations, seasons, cover vegetation and management conditions (Kato and Kamichika, 2006; Petry et al., 2024; Segovia-Cardozo et al., 2022). Therefore, tabulated crop coefficients in FAO-56 must be adjusted to reflect the specific growing conditions based on actual local *ET* measurements.

Kiwifruit (*Actinidia chinensis* deliciosa) and citrus (*Citrus reticulata* Blanco) are important perennial cash crops, and the area has increased rapidly because of the higher economic value and suitable climate in Southwest China (Chen et al., 2023; Jiang et al., 2022b). Despite the significant rainfall in Southwest China, the uneven distribution of rainfall over time causes the seasonal dry in spring and autumn, resulting in unstable agricultural production (Chen et al., 2023). Therefore, accurately calibrated crop coefficients and determined water use requirements are urgently required for optimizing agricultural water management and water resource reallocation. The objectives of our research were to (1) study the seasonal variations in energy and water fluxes in kiwifruit and citrus widely planted in this region, (2) determine the local K_c and K_{cb} curves based on actual *ET* and *T* measurements, and (3) analyze how the K_c and K_{cb} were regulated by the biophysical variables. This study provides one of the first comprehensive, long-term datasets combining EC and sap flow measurements to calibrate and validate both single and basal crop coefficients for drip-irrigated kiwifruit and citrus orchards in a humid subtropical climate. This addresses a critical gap in the literature, which has predominantly focused on field crops in arid and semi-arid regions, and offers directly applicable parameters for improving irrigation water management in similar humid hilly areas of Southwest China.

2. Materials and methods

2.1. Study region and site descriptions

The study area is located in the western Sichuan Basin, China, characterized by a subtropical monsoon humid climate (AM) according to the Köppen classification. It experiences a mean annual temperature of 16.5℃, annual precipitation of 1100 mm, a limited sunshine duration of 1122 h per year, and a high relative humidity of 82 %. The total amount of precipitation is generally sufficient for crop water consumption, with > 70 % of MAP occurring during the wet season (May-October). However, a lack of rainfall in autumn and spring can easily result in crop water shortages.

In our study, two orchard ecosystems, kiwifruit and citrus, were selected and fully instrumented to enable the state-of-the-art measurements of CO_2 and H_2O fluxes and meteorological variables. The geographical location, elevation, crop species, and physical soil properties of the two orchard sites are detailed in Table 1. Kiwifruit (*Actinidia chinensis* deliciosa cv. Jin Yan) and citrus (*Citrus reticulata* Hort. ex Tanaka) were planted in Pujiang and Qionglai sites, having the growing seasons of mid-March to the end of October for kiwifruit, and early April to mid-November for citrus. Winter pruning of fruit trees is usually carried out in January and February. The specific divisions of the different crop growth stages are outlined in Table 2. Kiwifruit was planted in the Pujiang site in 2006, with a spacing of 5.0 × 4.5 m, and began fruiting in 2009. The main trunk of the kiwi usually retains two branches, and sprigs on the branches are fixed, causing a canopy height of 1.8 m above the ground because of the implementation of a trellis system. The predominant soil type at the Pujiang site was yellow, with an average bulk density of 1.35 g cm^{-3}. The soil was composed of 76.8 % silt, 12.3 % sand, and 10.9 % clay. Citrus trees were planted at the

Table 1
Experimental site location, crop and soil parameters in the selected kiwifruit and citrus orchard.

Site information	Pujiang	Qionglai
Study period	2018–2020	2020–2023
Latitude (°N)	30.3265 N	30.3376°N
Longitude (°E)	103.4252E	103.4386°E
Elevation (m)	537	535
Mean annual temperature (°C)	16.3	17.5
Mean annual precipitation (mm)	1197	1117
Crop types	Kiwifruit	Citrus
Plant density (number/hm^2)	445	833
Maximum canopy height (m)	2.2	1.8
Maximum canopy leaf area index (m^2/m^2)	3.8	2.85
Soil type	Yellow loam	Yellow loam
Dry bulk density of soil (g cm^{-3})	1.35	1.15
Saturated volumetrical soil water content (θ_s, %)	47.1 %	45.2 %
Field capacity (θ_f, %)	33.5 %	30.8 %

Table 2
Duration and growing stages division of the kiwifruit and citrus orchard in Southwest China.

Crop types	Division	Initial	Developed	Middle	Late	Accumulated values
Kiwi	Days	27	25	98	70	220
	Date	15.Mar–10.Apri	11.Apri–5.May	6.May–11.Aug	12.Aug–20.Oct	
	GDD (℃)	344	540	1829	1095	3808
Citrus	Days	30	46	92	61	229
	Date	1.April–30.Apri	1.May–15.Jun	16.Jun–15.Sep	16.Sep–15.Nov	
	GDD (℃)	187	467	1216	357	2227

Note: GDD is growing degree days observed during the experimental period (℃).

Qionglai site since early 2018, with a spacing of 3.0 × 4.0 m and started fruiting in 2020. The canopy amplitude of citrus trees around the EC tower is measured by a meter stick during the observed period. Citrus trees typically have a canopy height ranging from 1.5 to 2.0 m and a canopy cover fraction up to 0.33. Notably, these two orchards were seasonally covered with wild grass beneath the tree canopy in kiwifruit and in the adjacent inner canopy in the citrus orchard. Farmers often allow grass growth in the orchard as it helps to mitigate soil erosion, boosts soil organic matter, and regulates soil and micrometeorology conditions. Both orchards are irrigated with surface water using the drip irrigation system. The irrigation water from the Dongfeng Canal irrigation district flows through the experimental orchards via the water conveyance channel. The local ecological environment bureau conducts regular water sampling from drainage channels to monitor water quality parameters, ensuring compliance with established irrigation water standards. The farmer uses a water pump to divert the water from the irrigation channel into the pond for backup. When irrigation is needed, the irrigation water passes through the backwashing sand and gravel filter, the disc filter and the irrigation pipeline in sequence, and is finally carried out by the dripper. In Pujiang, drippers delivered 1.6 L/hour, while they delivered 2.0 L/hour at 0.3 m intervals in the Qionglai experimental orchard. Irrigation was applied only when the soil water content dropped below 70 % θ_f, with the irrigation upper threshold set at 85 % θ_f. Irrigation amount was calculated as follows:

$$m = 1000 Z_r p(\beta_1 - \beta_2)\theta_f \quad (1)$$

Where m is the irrigation amount (mm); Z_r is the root depth (0.6 m); θ_f is the field capacity (g cm^{-3}); β_1 and β_2 represent 85 % θ_f and 70 % θ_f, respectively; p is the wetting ratio (50 %).

2.2. Field observations and data processing

2.2.1. EC measurements and data processing

In the center of each experimental site, the EC system was used to continuously measure latent heat (*LE*) and sensible heat (*H*) fluxes during the kiwifruit growing season of 2018–2020 and the citrus growing seasons of 2020–2023. The *EC* system consists of a 3D Sonic Anemometer (Campbell Scientific Inc., USA, model CSAT3) to measure three-dimensional wind speed and sonic air temperature, and a closed-

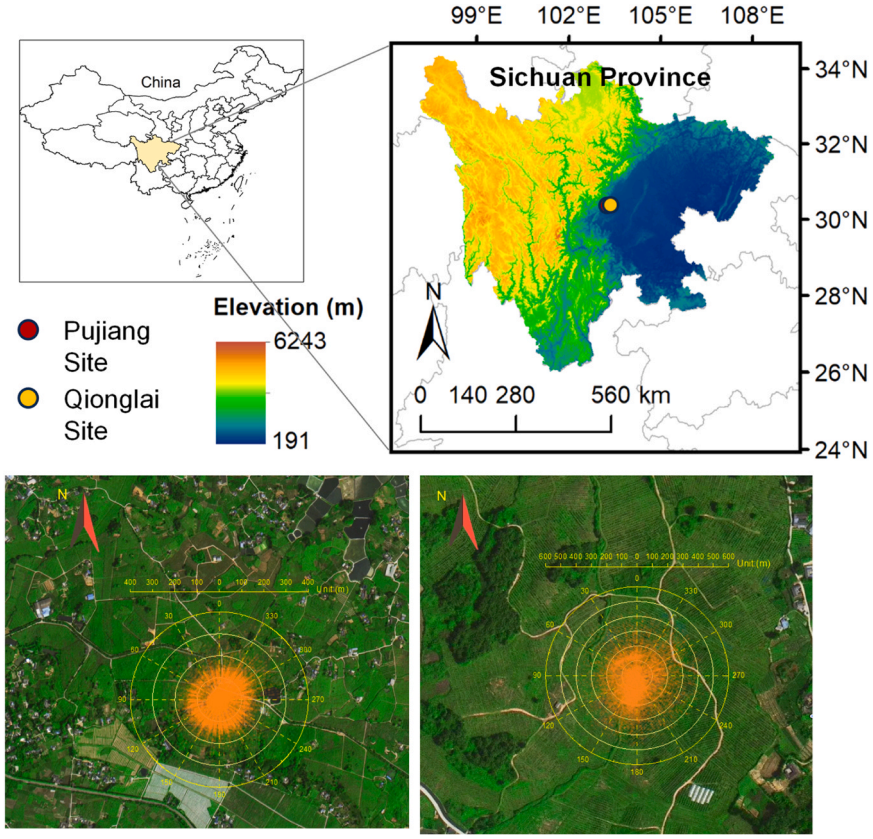

Fig. 1. The geographical location and overview of the studied ecosystems and the footprint for 90 % of effective fetch during the kiwi (left) and citrus (right) growing seasons. Imagery from Date 4 April 2022. Image from OvitalMap (V9.7.1) (www.ovital.com, Copyright 2010–2024 © Beijing Ovital Software Co., Ltd. All rights reserved).

path CO_2/H_2O gas analyzer sensors (EC155, Campbell Scientific Inc., USA) were installed at 8.0 m above the ground in Pujiang experimental site. During the observed period, 90 % of the effective fetch for the half-hour footprint was within 240 meters of the Pujiang EC site, while the nearest village was over 600 m away (Fig. 1). Therefore, the planting area was sufficiently large to provide an adequate fetch for both EC systems. While in the Qionglai experimental site, an open-path CO_2/H_2O gas analyzer sensors (EC150&CSAT3A, Campbell Scientific Inc., USA) were installed at 5.0 m above the ground to continuously measure citrus orchard *LE* and *H*. Citrus is grown within 500 m in any direction with the flux tower as the center of the circle (Fig. 1), which allowed us to neglect heat advection in the citrus field. *LE* and *H* were calculated by eddy covariance :

$$LE = \lambda \rho_a \overline{w'q'} \tag{2}$$

$$H = C_p \rho_a \overline{w'T'} \tag{3}$$

Where *LE* and *H* are the latent and sensible heat flux, respectively, (W m^{-2}); λ is the latent heat of vaporization, (J kg^{-1}); ρ_a is the moist air density, (kg m^{-3}); C_p is the specific heat at constant pressure (J kg^{-1} K^{-1}); $\overline{w'q'}$ indicates means of the products of the instantaneous deviation of vertical wind velocity w'(m s^{-1}) and air humidity q' from average (kg kg^{-1}) over certain time, 30 min in this study; $\overline{w'T'}$ indicates means of the products of the instantaneous deviation of vertical wind velocity w' and potential temperature T' from average (K) over 30 min.

To assure good quality control of the EC data, the original 10 Hz flux data were processed with the EddyPro software following standard procedures, including double-coordinate rotation, both low- and high-frequency corrections, time lag compensation for the closed-path gas analyzer, WPL density corrections for open-path system, etc., (Falge et al., 2001). Data were collected and averaged at 30 min using Datalogger Support Software version 4.4 (Campbell Scientific Inc., USA). Quality control of the half-hourly flux data was performed based on the quality flag provided by the calculation procedures, and the low-quality data were removed as described by Jiang et al. (2022b). For the missed and unreliable data, the linear interpolation method was used to fill the gaps that were less than 2 h, whereas larger gaps (>2 h) were filled using the daily average variation method introduced by Reichstein et al. (2005). For the longer gaps (15 days) that occurred in Qionglai owing to electricity interruption and maintenance, a backpropagation neural network (BP) model was used to estimate the missing water flux data. The BP model can automatically learn the complex mapping relationships between the input and output, enabling the modeling and prediction of nonlinear data using a backpropagation algorithm. Specifically, to minimize the potential influence of citrus phenological variations on the data imputation process, the BP model training incorporated data from both the period preceding the missing records and the subsequent 15 days. A total of 2880 half-hourly data sequences were used to train the BP neural network, with net radiation, wind speed, soil moisture, vapor pressure deficit, and air temperature as input variables, and *LE* as the output. The model achieved a training performance, with an R^2 of 0.87 and an *RMSE* of 3.87 W m^{-2}. Furthermore, the trained model was validated using independently collected data from a corresponding non-missing period, yielding a validation performance with R^2 of 0.84 and *RMSE* of 3.98 W m^{-2}. These results indicate that the BP neural network method provides reasonably reliable imputations for the half-hourly *LE* fluxes.

2.2.2. Meteorological and soil water content measurements

Meteorological measurements are taken over the irrigated orchard ecosystem, adjacent to the EC system, and the planting area is sufficiently large to provide an adequate fetch for meteorological measurements. Auxiliary meteorological variables, including air temperature (T_a, ℃), relative humidity (*RH*, %), precipitation (*P*, mm), net radiation (R_n, W m^{-2}), wind speed (*u*, m s^{-1}) and direction (*WD*, °), air pressure (P_a, KPa), soil temperature (T_s), soil moisture profile (*SWC*, %) and soil heat flux (*G*, W m^{-2}), were recorded every 30 min using sensors integrated with an EC system in Qionglai or independent automatic weather station in Pujiang site, the specific sensors and measurement location at each site are detailed in Table 3. The measured *u* was adjusted to 2 m reference height (u_2) using the wind speed profile equation for calculating ET_o (Allen et al., 1998). The auxiliary meteorological data were downloaded every two weeks, and the sensors were well supervised and maintained, including cleaning and calibrating for clean and level maintenance every two weeks. Four SWC sensors, with a measured interval of 0.2 m, were installed in a kiwifruit orchard (Table 3). Three SWC sensors were installed in the mid-row for measuring 0–0.50 m SWC, while ten SWC sensors, with the measured interval of 0.1 m, were installed in citrus plantation lines to obtain the citrus root zone SWC profile. This dual-location measurement strategy was implemented to capture the pronounced spatial heterogeneity in soil moisture inherent to drip-irrigated orchards with wide rows. The plantation line sensors monitored soil water dynamics in the primary root zone and wetted area under the drippers, which is most critical for plant water uptake. The mid-row sensors quantified moisture changes in the exposed, predominantly rain-fed inter-row space, which dominates *E*. For the calculation of the root zone depletion and the subsequent water stress coefficient (Eqs. 10–12), a soil-water-content-weighted average from the plantation line profile (representing the tree root zone) was used, as this directly reflects the water available for *T*. The *SWC* measured by sensors was calibrated using the gravimetric method with soil samples collected adjacent to the sensors. The quality of the measured data was evaluated by the built-in procedures, including the evaluation of the normal operation of the meteorological and soil water sensors and the reliability of the data test, and the accuracy of the datalogger clock time verification. Furthermore, the measured R_n data were evaluated against the estimated values derived from standard FAO-56 calculations (Allen et al., 1998) to determine the necessity for instrument recalibration. As T_a, *u*, *RH*, *G*, and *SWC* were measured at different positions, the simple visual method (trend analysis, consistency analysis) was used to assess whether one was faulty and reliable (ASCE-EWRI, 2005).

2.2.3. Ancillary crop parameter measurements

Eight sample plots were randomly selected every 1–2 weeks for measuring canopy leaf area index (LAI_c) with a leaf meter (LAI-2000, Li-Cor, inc. USA), covering the double rows and the space between two adjacent double rows, following the recommendations for row crops. Seasonal grass cover under the tree canopy and adjacent inter-canopy adds complexity to the orchard surface. MODIS-based vegetation parameters provided feasible ways for regional vegetation growth information investigation because of their availability and reliability (Kalfas et al., 2011; Huang et al., 2022). In this study, orchard total surface leaf area index (LAI_t) was obtained every eight days using the MODIS 15A2H reflectance product, which has a spatial resolution of 500 × 500 m (https://modis.ornl.gov/data.html). The data from the EC site's location was utilized. Linear interpolation of adjacent available data over time was used to fill the data gaps. The TIMESAT software was utilized to smooth spikes in the raw LAI data (Jonsson and Eklundh, 2004). Then, the eight-day LAI_t data were interpolated to a daily scale using a spline function.

The kiwi canopy amplitude measured approximately 5.0 × 3.5 m, with a maximum cover fraction of 0.8 during the mid-season, estimated based on the Beer–Lambert law. The canopy of citrus is evergreen, and the canopy cover fraction was estimated based on citrus canopy amplitude and actual occupying space (3.0 × 4.0 m).

2.2.4. Sap flow measurements and data processing

Stem sap flux was assessed via the Granier heater dissipation method and then upscaled to determine the orchard's total *T* (Granier, 1987). The sap flow technique employed a pair of heated and unheated needles inserted into the trunk to sample the conductive area, the heat in the

Table 3
Instrumentation and environmental variables of observed orchard sites.

Parameter	Sites	Instruments and manufacture	Installed height or depth (m)
Air temperature and Relative humidity	Pujiang	HPM155, Vaisala, Helsinki, Finland	8.0
	Qionglai	HMP155, Vaisala, Finland	4.0
Precipitation	Pujiang	L3, Jinzhou Sunshine Meteorological Technology CO., LTD., Jinzhou, CN	0.6
	Qionglai	RG13 H2NN, Vaisala, Finland	2.0
Solar radiation	Pujiang	TBQ−2, Jinzhou Sunshine Meteorological Technology CO., LTD., Jinzhou, CN	3.5
	Qionglai	NR01, Hukseflux, Netherlands	4.0
Net radiation	Pujiang	TBB−1, Jinzhou Sunshine Meteorological Technology CO., LTD., Jinzhou, CN	3.5
	Qionglai	NR01, Hukseflux, Netherlands	4.0
Soil heat flux	Pujiang	HP−1, Jinzhou Sunshine Meteorological Technology CO., LTD., Jinzhou, CN	2 layers (−0.05, −0.10)
	Qionglai	HFP01, Hukseflux, Netherlands	4 layers (−0.05, −0.1, −0.15, −0.2)
Soil temperature	Pujiang	PTWD−2A, Jinzhou Sunshine Meteorological Technology CO., LTD., Jinzhou, CN	4 layers (−0.05, −0.1, −0.15, −0.2)
	Qionglai	CS655, Campbell, USA	3 layers (−0.05, −0.1, −0.2)
Soil volumetric water content	Pujiang	TDR−3, Jinzhou Sunshine Meteorological Technology CO., LTD., Jinzhou, CN	4 layers (−0.2, −0.4, −0.6, −0.8) between the lines and rows
	Qionglai	CS655, Campbell, USA	3 layers (−0.15, −0.30, −0.45) between the lines 10 layers (−0.1, −0.2, −0.3, −0.4, −0.5, −0.6, −0.7, −0.8, −0.9, −1.0) between the rows

upper probe was dissipated into the sapwood to measure the vertical sap flux surrounding the probe. Eight trees within the flux footprint of EC were selected as the experimental trees for plant sap flux measurement, with an installed height of 0.60 m above the ground for kiwifruit. Although prior studies have proved that different sap flow rates within the trunk, with the sunny side often overestimating the average flow rates (Molina et al., 2016; Flo et al., 2019). In this study, the kiwi vines were uniformly fixed by iron wires at a height of 1.8 m, causing a horizontal canopy structural feature, the sap flow difference between the north and south-facing sides was ignored due to the relatively uniform distribution of sunlight within the canopy (Jiang et al., 2022). Since the citrus tree canopy was vertical, and apparent sunny leaves and shaded canopy existed between the north or south-facing side, therefore, eight citrus trees were selected for sap flow measurement, with four sensors installed on the south/north-facing side of the tree at 0.30 m above the ground, and the averaged value was used to calculate sap flow. Sensor calibration, including zero offset without sap flow, needle distance calibration, response time and frequency calibration, was made before installation. Besides, to minimize potential measurement errors caused by solar radiation, rainfall, and natural thermal gradients, the trunk area where the sap flow sensors were installed was fully covered with sunscreen film. After installation, the needles are insulated with reflecting materials. The sap flux density (J_S (g H_2O m^{-2} s^{-1})) was determined by measuring the temperature difference between heated and unheated samples.

$$J_s = a\left[\frac{\Delta T_{max} - \Delta T}{\Delta T}\right]^b \quad (4)$$

Where a and b are the empirical coefficients, which were 119 and 1.231 for this study. ΔT_{max} denotes the maximum temperature difference observed when sap flux is zero, defined as the daily maximum temperature difference (℃). ΔT represents the temperature difference between heated and unheated needles. Sap flow fluxes were calculated by multiplying the J_S with the sapwood area (Granier, 1987). The selected sample trees were located within 0.5 km of the EC tower at each site. The stem sap flow was estimated every 10 min based on original measurements. These data were subsequently extrapolated to estimate single tree canopy scale T using Eq. (5):

$$T = J_s\frac{A_s}{A_g} \quad (5)$$

Where J_S (g H_2O m^{-2} s^{-1}) represents the sap flux per unit xylem area, with A_s denotes the average xylem section area, and A_g denotes the ground area per tree. Eight sample trees were selected for sap flow installation purposes in both orchard sites, while the number may not represent the average growth level of experimental trees. As sap flow measurements are plant-based processes, more than 30 trees were collected randomly to investigate measurement representativeness and estimate conductive xylem area. Sample trees were obtained within a 0.5 km × 0.5 km plot centered around the tower. Sapwood thickness of each sample tree was measured using a core extracted with a 5-mm increment borer. The heartwood area depth was determined by its unique color variations. The canopy T of the sampled trees was averaged to estimate the ecosystem T at the kiwifruit and citrus tree sites.

2.2.5. Consideration of measurement uncertainties

The derived crop coefficients are subject to uncertainties originating from the measurement techniques. For the EC system, the energy balance closure was 0.92 and 1.04 for the kiwifruit and citrus sites, respectively (Table 5), and gap-filling for missing ET data introduced additional uncertainty, though higher accuracy (R^2 of 0.84 and *RMSE* of 3.98 W m^{-2}) for the neural network model used in the citrus site inspires confidence.

In sap flow measurements, potential uncertainties arise from the spatial variability of sap velocity within trees and the scaling from point measurements to stand-level transpiration. This is because sap flow rates are rarely uniform across the sapwood area, as conducting properties were different along the xylem radial direction (Flo et al., 2019). We mitigated this by sampling multiple trees and sides (for citrus) and using a large sample size (>30 trees) to characterize the sapwood area. Furthermore, the wound effect caused by the invasive measurement may also result in uniform thermal diffusion gradients (Wiedemann et al., 2016). Due to the lack of direct measurement data for theoretical sap flow correction, the T of kiwifruit and citrus provided in this study may slightly deviate from the actual values. However, the systematic application of standardized sensor placement protocols across all study trees ensured measurement consistency, and inter-annual trends exhibited strong temporal stability.

2.3. Calculation of reference evapotranspiration and crop coefficient

According to FAO-56, crop actual ET (ET_a) can be estimated using the crop coefficient (single K_c and dual K_c, reflecting the specific

characteristics of the crop), and ET_o, as recommended by Allen et al. (1998). It is critically acknowledged that the standardized parameters of the ET_o calculation equation (e.g., the fixed surface resistance of 70 s m^{-1} and the aerodynamic resistance parameterization) are explicitly defined for a well-watered hypothetical grass surface. In this study, however, the required meteorological data were measured within the orchard, which presents different surface characteristics. Therefore, the ET_o values estimated here represent the ET demand for the hypothetical grass reference surface under the specific local microclimatic conditions of the experimental orchard. This approach, while deviating from the ideal scenario, is consistent with the practical recommendations of FAO-56 when site-specific weather data from a reference surface are unavailable (Allen et al., 1998). It was adopted to ensure internal consistency in our modeling and, most importantly, to accurately capture the microclimatic drivers that a distant standard weather station might not represent (Jamshidi et al., 2020; Peddinti and Kambhammettu, 2019; Wang et al., 2020). This site-specific ET_o estimate is considered more appropriate for assessing the actual atmospheric water demand experienced by the specific crop at the study site.

$$ET_a = K_s K_c ET_o = (K_s K_{cb} + K_e) ET_o \tag{6}$$

$$ET_o = \frac{0.408\Delta(R_n - G) + \gamma \frac{900}{T_{mean}+273} u_2 (e_s - e_a)}{\Delta + \gamma(1 + 0.34u_2)} \tag{7}$$

Where $\Delta$is the curve slope of the saturation vapor pressure (kPa $℃^{-1}$), γ is the psychrometric constant (KPa $℃^{-1}$), T_{mean} is the mean air temperature (℃), e_s and e_a represent the saturated and actual water vapor pressure (kPa), respectively. K_{cb} is the basal crop coefficient; K_e is the soil evaporation coefficient. According to the dual K_c approach, K_{cb} can be derived based on the measured T in the orchard ecosystem.

$$K_{c-derived} = ET_a / ET_o / K_s \tag{8}$$

$$K_{cb-derived} = T / ET_o / K_s \tag{9}$$

Where K_s is the water stress coefficient, the detailed calculations are available in Allen et al. (1998).

$$K_s = \begin{cases} \frac{TAW - D_{r,i}}{TAW - RAW} = \frac{TAW - D_{r,i}}{(1-\rho)TAW}, & D_{r,i} > RAW \\ 1, & D_{r,i} \le RAW \end{cases} \tag{10}$$

Where TAW is the total soil water accessible to crops within the effective root zone, determined by the difference between the water content at field capacity (θ_f) and the wilting point (θ_{wp}) (Allen et al. 1998). ρ represents the portion of TAW that a crop can extract from the root zone before suffering water stress.

$$D_{r,i} = D_{r,i-1} - (P_i - RO_i) - I_i - CR_i + ET_{c,i} + DP_i \tag{11}$$

$$D_{r,i-1} = 1000(\theta_i - \theta_{i-1}) Z_r \tag{12}$$

Where $D_{r,i}$ is root zone depletion (mm), the subscript i denotes the day of i. $D_{r,i-1}$ is the water content in the root zone (mm), P_i is the precipitation (mm), RO_i is the runoff from the soil surface (mm), I_i is the net irrigation depth that infiltrates the soil (mm), CR_i is the capillary rise from the groundwater table (mm), $ET_{c,i}$ is the crop evapotranspiration (mm), DP_i is the water loss out of the root zone by deep percolation (mm). RO_i was estimated based on the measured drainage volume of the drainage ditch and the drainage area. θ_i and θ_{i-1} denotes the soil water content in the day of i and i-1. Z_r is the root depth (mm). The groundwater table for the experimental site was 10–13 m below the ground, CR_i and DP_i can be negligible in this study according to Allen et al. (1998). The seasonal water balance showed that the water depth of RO+ET+D_r was overall consistent with the variations of $P + I$ during the growing seasons for both orchard sites. The calculated relative bias (calculated as abs [(RO+ET+D_r)-($P + I$)]/($P + I$)) between RO+ET+D_r and $P + I$ was 27.0, 12.9, 9.7 and 15.7 % during the growing seasons of 2020–2023 in citrus sites, while the values was 20.3, 16.3 and 15.2 % during the 2018–2020 growing seasons for kiwifruit site, respectively. The seasonal water balance and the cumulative water volume of different water cycle components in the orchards during the growing season can be found in Fig. S1 and S2.

$$TAW = 1000(\theta_f - \theta_{wp}) Z_r \tag{13}$$

$$\rho = \rho_{table} + 0.04(5 - ET_c) \tag{14}$$

$$RAW = \rho TAW \tag{15}$$

Where ρ_{table} is referred as 0.35 for kiwifruit and 0.50 for citrus, respectively.

The FAO-56 method provides standardized K_c values for various growth stages under standard conditions (u_2 = 2 m s^{-1} and RH_{min} = 45 %). The single-crop coefficient K_c is defined by three distinct values: $K_{c\text{-ini}}$, $K_{c\text{-mid}}$, and $K_{c\text{-end}}$, corresponding to the K_c at the initial, mid-season, and late-season stages, respectively (Allen et al., 1998). According to FAO-56, the tabulated K_c values have to be adjusted into a local K_c by considering the crop-specific effects of relative humidity, wind speed and crop characteristics. $K_{c\text{-ini}}$ can be modified according to the mean interval between wetting events and evaporation rate, while $K_{c\text{-mid}}$ and $K_{c\text{-end}}$ were adjusted based on u_2, RH_{min} and crop height (h). For sparse vegetation, as vegetation having stand characteristics compared to 'pristine' conditions, like citrus planted in a wide row, the adjustment equation should consider the effect of cover fraction as presented in Eq. (17):

$$K_{c-FAO56adj} = K_{c-FAO56table} + [0.04(u_2 - 2) - 0.004(RH_{min} - 45)] \left(\frac{h}{3}\right)^{0.3} \tag{16}$$

$$K_{cb-FAO56adj} = K_{cmin} + (K_{cb\ full} - K_{cmin})(1 - \exp[-0.7LAI_c]) \tag{17}$$

$$K_{cbfull} = K_{cb-FAO56table} + [0.04(u_2 - 2) - 0.004(RH_{min} - 45)] \left(\frac{h}{3}\right)^{0.3} \tag{18}$$

Where $K_{c\text{-FAO56 adj}}$ and $K_{cb\text{-FAO56 adj}}$ represent the adjusted K_c and K_{cb} considering the local environment conditions. $K_{c\ min}$ represents the minimum K_c for bare soil, typically ranging from 0.15 to 0.20, $K_{cb\ full}$ denotes the estimated basal K_{cb} during the mid-season for vegetation with complete ground cover. $K_{c\text{-FAO56 table}}$ and $K_{cb\text{-FAO56 table}}$ represent the tabulated values of K_c or K_{cb} as outlined in the FAO report (Allen et al., 1998). In this study, $K_{c\text{-FAO56 table}}$ and $K_{cb\text{-FAO56 table}}$ for kiwifruit and citrus were calculated combined with the values under active ground cover and no active ground cover.

$$K_{c-FAO56table} = f_c K_{cngc} + (1 - f_c) K_{ccover} \tag{19}$$

$$K_{cb-FAO56table} = f_c K_{cb\ ngc} + (1 - f_c) K_{cb\ cover} \tag{20}$$

where $K_{c\ ngc}$ ($K_{cb\ ngc}$) is the K_c (K_{cb}) of citrus and kiwifruit with no active ground cover, $K_{c\ cover}$ ($K_{cb\ cover}$) is the K_c (K_{cb}) for the active ground cover (0.95, (0.90)), f_c is the fraction of ground covered by tree canopy (e.g., the sun is presumed to be directly overhead). For humid and subhumid climates, where there is less stomatal control by citrus, values for $K_{c\ ini}$ ($K_{cb\ ini}$), $K_{c\ mid}$ ($K_{cb\ mid}$), and $K_{c\ end}$ ($K_{cb\ end}$) were increased by 0.1, 0.2 and 0.2 following Rogers et al. (1983).

The derived K_c ($K_{c\text{-derived}}$) or K_{cb} ($K_{c\text{-derived}}$) multiplied by K_s is regarded as the local actual K_c ($K_{c\text{-local}}$) or K_{cb} ($K_{cb\text{-local}}$), which is an adjusted recommended value based on the water availability and local climatic conditions. The standard, transferable K_c ($K_{c\text{-standard}}$) and K_{cb} ($K_{cb\text{-standard}}$) values are applicable for irrigation management and precipitation frequencies typical of a sub-humid climate with RH_{min} = 45 %

and $u_2 = 2$ m s^{-1} (Allen et al., 1998). When local climatic conditions differ from these meteorological values, the derived K_c and K_{cb} values, need to be adjusted by atmosphere correction to become the $K_{c\text{-standard}}$ or $K_{cb\text{-standard}}$ values for transferable purposes. In our study, $K_{c\text{-standard}}$ and $K_{cb\text{-standard}}$ values were calculated based on $K_{c\text{-derived}}$ and $K_{cb\text{-derived}}$, respectively.

$$K_{c-standard} = K_{c-derived} - [0.04(u_2 - 2) - 0.004(RH_{\min} - 45)]\left(\frac{h}{3}\right)^{0.3} \quad (21)$$

$$K_{cb-standard} = K_{cb-derived} - [0.04(u_2 - 2) - 0.004(RH_{\min} - 45)]\left(\frac{h}{3}\right)^{0.3} \quad (22)$$

2.4. Calculation of underlying conductance (G_s) and growing degree days (GDD)

To determine the relationship between $K_{c\text{-local}}$, $K_{cb\text{-local}}$ and underlying characteristics in various croplands, the underlying conductance (G_s) was calculated as follows (Monteith, 1965):

$$G_s = \frac{LE \cdot G_a}{\frac{\Delta}{\gamma}(R_n - G) - \left(\frac{\Delta}{\gamma} + 1\right)LE + \frac{\rho_a \cdot c_p \cdot VPD \cdot G_a}{\gamma LE}} \quad (23)$$

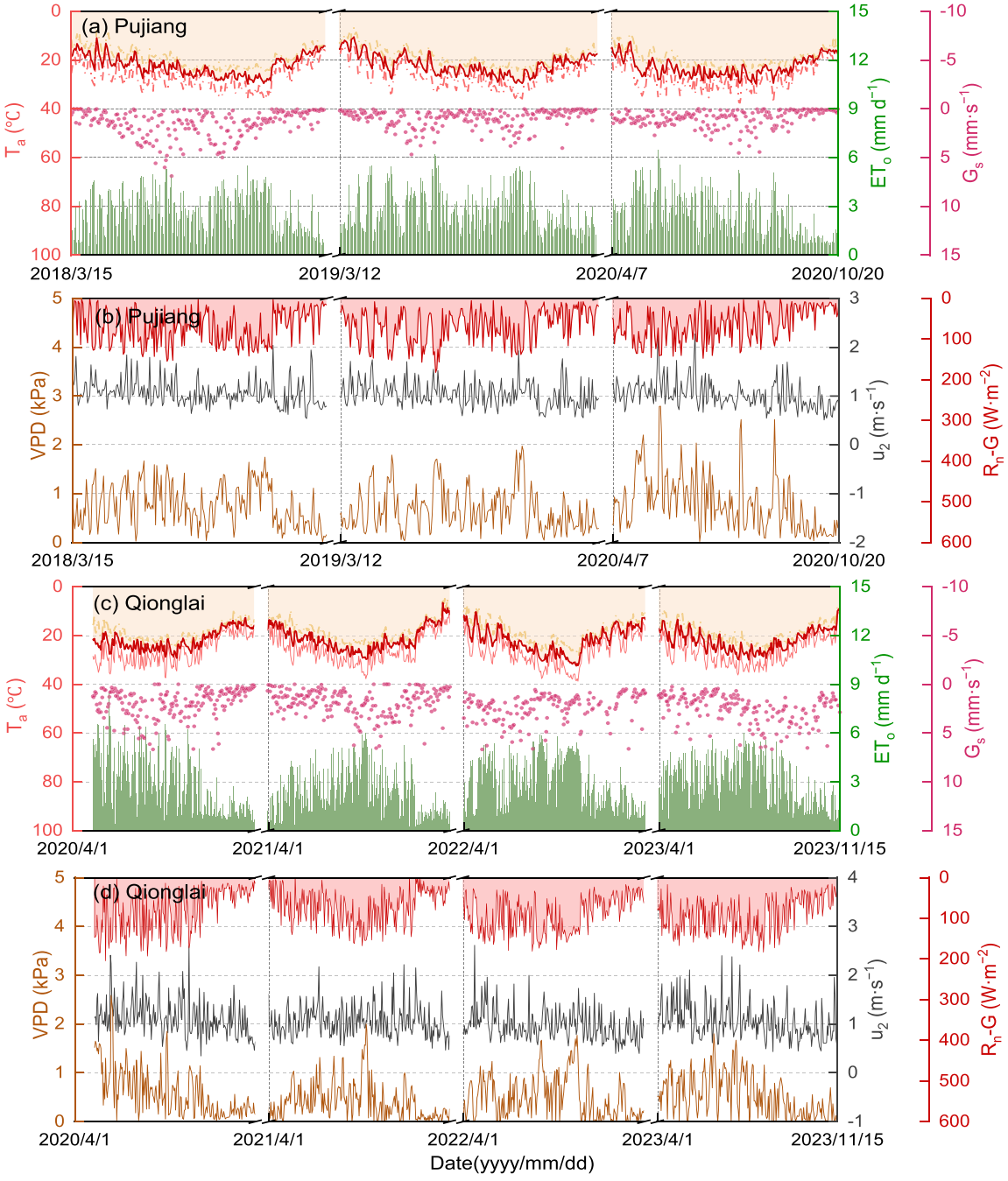

Fig. 2. Seasonal variations of biophysical factors in Pujiang and Qionglai cropland sites. Biophysical factors include daily average air temperature (T_a), daily maximum temperature ($T_{a\text{-max}}$), daily minimum temperature ($T_{a\text{-min}}$), reference crop evapotranspiration (ET_o), canopy conductance (G_s), vapor pressure deficit (VPD), wind speed at 2 m height (u_2), and daily available energy defined as net radiation reducing soil heat flux (R_n-G).

$$G_a = \frac{k^2 u}{\left[\ln\left(\frac{z_h - d}{z_{oh}}\right)\right]\left[\ln\left(\frac{z_m - d}{z_{om}}\right)\right]} \quad (24)$$

Where G_a is the aerodynamic conductance (s m^{-1}); z_h and z_m are the measured height of the wind speed, air temperature and relative humidity (m), respectively; and u is the measured wind speed (m s^{-1}); k is the von Karman constant (0.41). The momentum transfer roughness length, z_{om} is determined by the equation of $z_{om} = 0.13h_c$ (m); the heat transfer roughness length (z_{oh}), is given by $0.1z_{om}$; h_c is the mean canopy height of the crop (m); and the zero-plane displacement height (d, m), is calculated using the formula $d = 0.63h_c$.

GDD was calculated from the daily mean-temperature by subtracting base-temperature (T_{base}) and expressed in ℃ day, while T_{base} was set at 12 ℃ for citrus and 5 ℃ for kiwifruit (Kwon et al., 2021).

$$GDD = \left[\frac{(T_{max} - T_{min})}{2} - T_{base}\right] \quad (25)$$

Where T_{max} and T_{min} indicate the daily maximum and minimum air temperature, respectively. If the T_{max} is above the upper temperature value of 30 ℃, then 30 ℃ is used to replace T_{max} in Eq. (25). If (T_{max}-T_{min})<T_{base}, then the calculated *GDD* is recognized as zero on this day.

3. Results

3.1. Meteorological conditions

The seasonal variations in the meteorological variables, ET_o and G_s across the various growing seasons of the two orchard sites are shown in Fig. 2, and the average values of these factors at the individual stages and the entire growing season are summarized in Table 4. Given the varying growth periods, the average meteorological factors, ET_o and G_s observed during the mid-season stage were generally higher than those during the crop initial and late-season stages (Fig. 2, Table 4). All factors, except u_2, exhibited significant seasonal variations at the two experimental sites, with peak values generally occurring during summer (Fig. 2). Although the annual meteorological conditions were similar in the two sites, the crops experienced varying climatic conditions because of the different growing seasons at each location. For instance, the average T_a was 22.3℃ for kiwifruit in Pujiang, while the value was 21.8℃ for citrus in the Qionglai site (Table 4). Daily *VPD* and R_n were averaged at 0.74 kPa and 69.3 W m^{-2} for kiwifruit, 0.51 kPa and 89.9 W m^{-2} for citrus, respectively. The daily average u_2 values were comparable in the two sites, with a value of approximately 1 m s^{-1}. LAI_t showed seasonal variation in the two experimental orchards, and LAI_t was larger than LAI_c throughout the experimental period due to the presence of understory weed (Fig. S3 and S4). Differences in meteorological factors and phenological rhythms resulted in varying atmospheric evaporative demands between the crops, with ET_o values of 2.68 mm d^{-1} for kiwifruit at Pujiang, 2.79 ± 0.27 mm d^{-1} for citrus at the Qionglai site. The G_s consistently increased from the initial stage, peaked during the mid-season stage, and then gradually decreased.

3.2. Energy balance and seasonal variations

The relationship between R_n-G and $LE + H$ exhibited a significant linear correlation during the observational period (Fig. 3, $P < 0.01$). The slopes between daily R_n-G and $LE + H$ were estimated at 0.93 and 0.82 for kiwi and citrus orchard, with intercepts of −0.25 and 18.95 W m^{-2}, and coefficients of determination (R^2) of 0.85 and 0.90, respectively (Fig. 3, Table 5). The *EBC* ($EBC = \sum(LE + H)/\sum(R_n - G)$) values were estimated at 0.92 for the Pujiang and 1.04 for the Qionglai sites, suggesting a high reliability of the energy closure measurements (Cui and Chui, 2019; Wilson et al., 2002). The residual energy (*RE*, calculated as R_n-*G*-*LE*-*H*) was redistributed using the evaporative fraction (EF) method to achieve energy forced closure (Gebler et al., 2015). Specifically, EF was estimated based on the ratio of the sum of 15-day LE to the sum of LE+H, and the forced closure corrected *LE* (LE_{Corr}) was described as $LE_{Corr} = LE + RE \times EF$, LE_{Corr} was then used to calculate *ET* by dividing λ.

The average diurnal variations in R_n, *LE*, *H*, and *G* during the individual crop growth stages and throughout the growing season are illustrated in Fig. 4. The average diurnal energy fluxes showed an unimodal pattern during crop each growth stage and the entire growing season, with peaks generally occurring between 12:30 and 2:00. Both *LE* and *H* varied with R_n, with *LE* consistently higher than *H* throughout the growing season. The average daily energy fluxes reached their highest levels from the beginning to the mid-season stage, and then declined towards the late-season stage. The average R_n, *LE*, *H*, and *G* was 69.28 ± 4.84 (standard deviations), 53.04 ± 4.65, 15.14 ± 1.53, and 0.88 ± 0.39 W m^{-2} for kiwifruit, 89.87 ± 13.75, 64.59 ± 9.26, 20.39

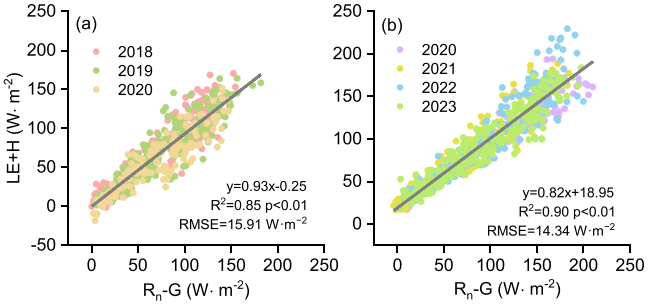

Fig. 3. Regression analysis of available energy (defined as the difference between net radiation (R_n) and soil heat flux (G)) and the sum of latent heat (*LE*) and sensible heat flux (*H*) in the (a) kiwifruit and (b) citrus orchard during the growing seasons.

Table 4
Averaged biophysical factors and reference evapotranspiration (ET_o, mm·d−1) at the different growth stages in the drip-irrigated kiwifruit and citrus orchard in Southwest China. Biophysical factors include air temperature (T_a, ℃), wind speed at 2 m height (u_2, m s^{-1}), water vapor deficit (*VPD*, kPa), net radiation (R_n, W m^{-2}), Precipitation (*P*, mm), underlying total leaf area index (LAI_t, m^2 m^{-2}).

Crop types	Stage	Days	*Ta*	*u2*	*VPD*	*Rn*	*P*	LAI_t	*ETo*
Kiwifruit	Ini	27	16.5	1.16	0.68	68.5	87.5	1.98	2.59
	Dev	35	20.3	1.11	0.87	82.1	123.2	2.58	3.03
	Mid	92	25.0	1.05	0.85	80.4	832.6	3.41	3.02
	Lat	66	21.5	0.95	0.55	47.2	277.2	3.04	2.05
	Average	220	22.3	1.04	0.74	69.3	1320.5	2.93	2.68
Citrus	Ini	30	17.9	1.14	0.54	94.0	69.3	1.41	2.84
	Dev	46	22.0	1.12	0.68	104.1	108.0	1.67	3.23
	Mid	92	25.6	1.08	0.62	111.5	578.7	1.67	3.41
	Lat	61	17.3	0.92	0.20	45.7	148.2	1.08	1.52
	Average	229	21.8	1.05	0.51	89.9	908.2	1.44	2.79

Note: underlying' total leaf area index, including tree canopy and grass leaf area.

Table 5
Energy components and regression analysis of energy balance closure (EBC) in the drip-irrigated kiwifruit and citrus orchard in Southwest China.

Crop	Year	*EBC*	y = a*x + b	R^2	*RMSE*	R_n (W·m−2)	LE_{Corr}	H_{Corr}	*G*
Kiwifruit	2018	0.98	y = 0.96x+ 2.47	0.87	15.29	71.38	54.02	16.68	0.63
	2019	0.88	y = 0.94x−0.64	0.85	16.52	71.12	49.75	20.04	1.32
	2020	0.80	y = 0.86x−1.14	0.86	14.07	69.14	49.02	19.41	0.71
	Average−3years	0.92	y = 0.93x−0.25	0.85	15.91	69.28 ± 4.84	53.04 ± 4.65	15.14 ± 1.53	0.88 ± 0.39
Citrus	2020	1.01	y = 0.77x+ 20.45	0.93	11.82	99.63	71.47	20.21	4.08
	2021	1.11	y = 0.83x+ 20.13	0.91	11.66	70.85	50.93	15.44	1.89
	2022	1.04	y = 0.90x+ 13.60	0.88	17.73	97.52	67.66	22.94	3.67
	2023	1.01	y = 0.79x+ 20.26	0.90	12.76	97.70	68.31	22.96	2.46
	Average−4years	1.04	y = 0.82x+ 18.59	0.90	13.59	89.87 ± 13.75	64.59 ± 9.26	20.39 ± 3.54	3.02 ± 1.02

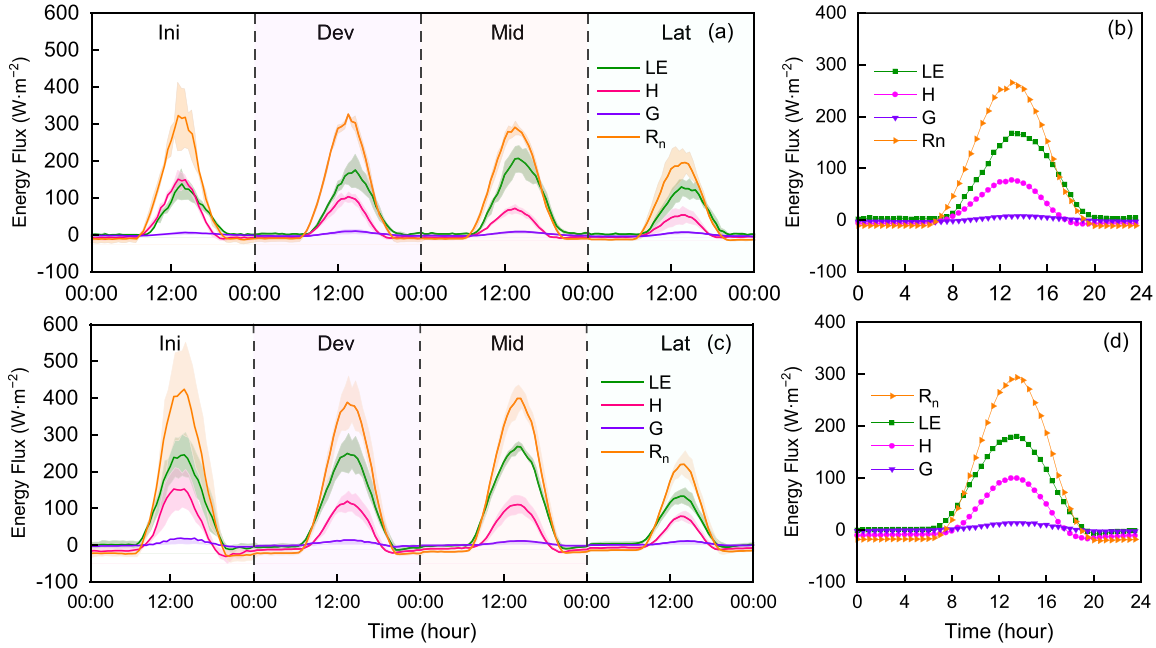

Fig. 4. Averaged diurnal variation of net radiation (R_n), latent heat flux (LE), sensible heat flux (H), and soil heat flux (G) at the kiwifruit (upper and a and b) and citrus (below c and d) individual growth stages (initial, developed, middle, and late growing stage, left) and total growing seasons (right).

± 3.54, and 3.02 ± 1.02 W m^{-2} for citrus, respectively (Table 5). The consistently low magnitude of the G relative to R_n, *LE*, and *H* is a typical feature of well-vegetated, closed-canopy ecosystems, where most of the available energy is partitioned into *LE* and *H* fluxes, with minimal energy reaching and being stored in the soil substrate (Wilson et al., 2002).

3.3. Seasonal variation in evapotranspiration, evaporation, and transpiration

The seasonal variations and statistical summarizations of the *ET* and its components in the two orchard sites are illustrated in Fig. 5 and Table 6. Daily *ET* and *T* showed similar variation patterns, which were relatively low in the initial stage, increased with crop canopy development and supported water and heat conditions during the mid-season stage, and showed a decreasing trend toward the late-season stage. The seasonal *T* exhibited a smaller variation amplitude than the corresponding *ET*. The differences between the two were more pronounced in summer, during periods of high atmospheric demand and abundant precipitation, and gradually decreased as the *ET* decreased (Fig. 5). The daily average *ET* and *T* were measured at 2.04 ± 0.18 mm d^{-1} and 1.15 ± 0.16 mm d^{-1} for kiwifruit in Pujiang, 2.49 ± 0.25 mm d^{-1} and 1.18 ± 0.09 mm d^{-1} for citrus in Qinglai site, respectively. *T* contributed approximately 50 % of the total *ET*, with specific ratios of 0.57 ± 0.02 for kiwifruit, 0.52 ± 0.05 for citrus, respectively.

As a difference between *ET* and *T*, daily *E* in kiwifruit increased from the initial and crop development stage, but decreased subsequently. However, the seasonal patterns of *E* in citrus croplands increased until the late-season stage. Furthermore, in comparison to *T*, daily *E* fluctuated sharply throughout the growing season in the two orchard sites, with the daily average of 0.89 ± 0.04 mm d^{-1} in kiwifruit and 1.31 ± 0.19 mm d^{-1} in the citrus orchard, respectively.

3.4. Seasonal variation of crop K_c and K_{cb}

The water stress coefficient (K_s) showed seasonal variability, with values below 1 occurring mainly during the initial and late-season stages when soil moisture was limited (Fig. S5). This reduction in K_s contributed to lower $K_{c\text{-local}}$ and $K_{cb\text{-local}}$ values during these periods, as proved in Fig. 6, a linear relationship was found between K_s, $K_{c\text{-local}}$, and $K_{cb\text{-local}}$ in both orchards. Daily K_c, K_{cb} values and the locally developed curves for kiwifruit and citrus are shown in Fig. 7 and Fig. 8. The locally derived kiwifruit K_c ($K_{c\text{-local}}$) and $K_{c\text{-standard}}$ values exhibited seasonal variations, which were both lower in the crop initial stage, tended to reach their maximum in the mid-season stage, and subsequently decreased during the late-season stage (Fig. 7). The initial $K_{c\text{-local}}$ for kiwifruit was 0.67 ± 0.01, which was higher than the corresponding staged $K_{c\text{-FAO56 table}}$ and $K_{c\text{-FAO56 adj}}$ values (0.40, 0.34 ± 0.01), while the values during the kiwifruit mid-season and late-season stages (0.89 ± 0.02 and 0.68 ± 0.02) were slightly lower than the corresponding staged $K_{c\text{-FAO56 table}}$ and $K_{c\text{-FAO56 adj}}$ values (Fig. 7 and Table 7). Kiwifruit $K_{cb\text{-local}}$ exhibited a

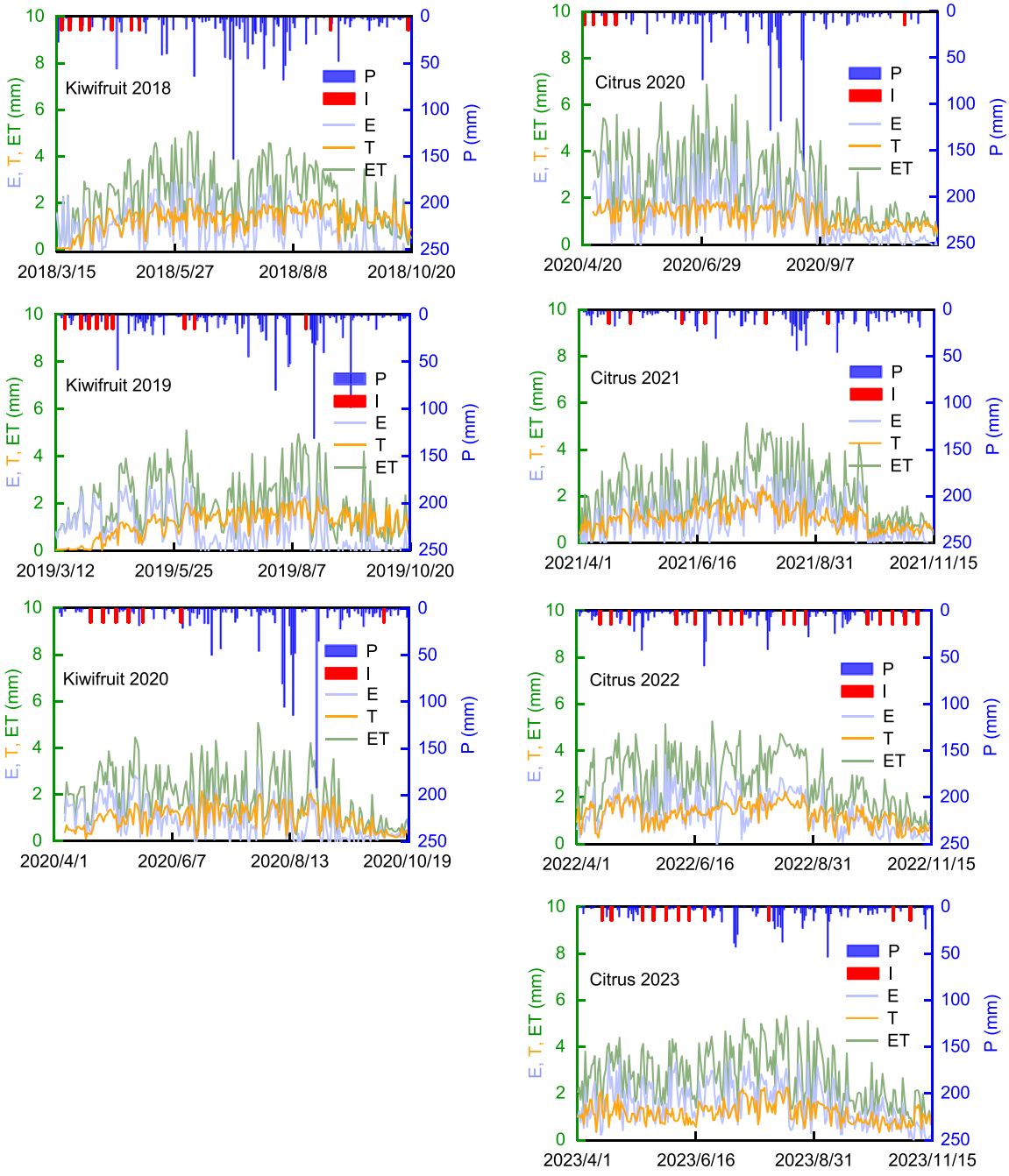

Fig. 5. Seasonal variations of precipitation (*P*), irrigation (*I*), evapotranspiration (*ET*), transpiration (*T*), and evaporation (*E*, defined as *ET*-*T*) in the kiwifruit and citrus orchard.

Table 6
Measured daily average evapotranspiration (*ET*, mm d^{-1}), transpiration (*T*, mm d^{-1}) and soil evaporation (*E*, mm d^{-1}) in the drip-irrigated kiwifruit and citrus orchard during the observed periods.

Crop types	Year	Stage	*ET*	*E*	*T*	*T*/*ET*
Kiwifruit	2018–2020	Ini	1.44 ± 0.31	1.10 ± 0.29	0.33 ± 0.20	0.24 ± 0.16
		Dev	2.28 ± 0.13	1.30 ± 0.14	0.98 ± 0.25	0.45 ± 0.10
		Mid	2.50 ± 0.24	1.12 ± 0.17	1.38 ± 0.14	0.61 ± 0.04
		Lat	1.47 ± 0.30	0.29 ± 0.09	1.18 ± 0.35	0.72 ± 0.10
		Seasonal	2.04 ± 0.18	0.89 ± 0.04	1.15 ± 0.16	0.57 ± 0.02
Citrus	2020–2023	Ini	2.42 ± 0.83	1.27 ± 0.55	1.15 ± 0.30	0.47 ± 0.05
		Dev	2.77 ± 0.50	1.57 ± 0.37	1.21 ± 0.20	0.47 ± 0.08
		Mid	3.12 ± 0.18	1.70 ± 0.15	1.42 ± 0.08	0.49 ± 0.03
		Lat	1.38 ± 0.24	0.57 ± 0.20	0.81 ± 0.08	0.63 ± 0.10
		Seasonal	2.49 ± 0.25	1.31 ± 0.19	1.18 ± 0.09	0.52 ± 0.05

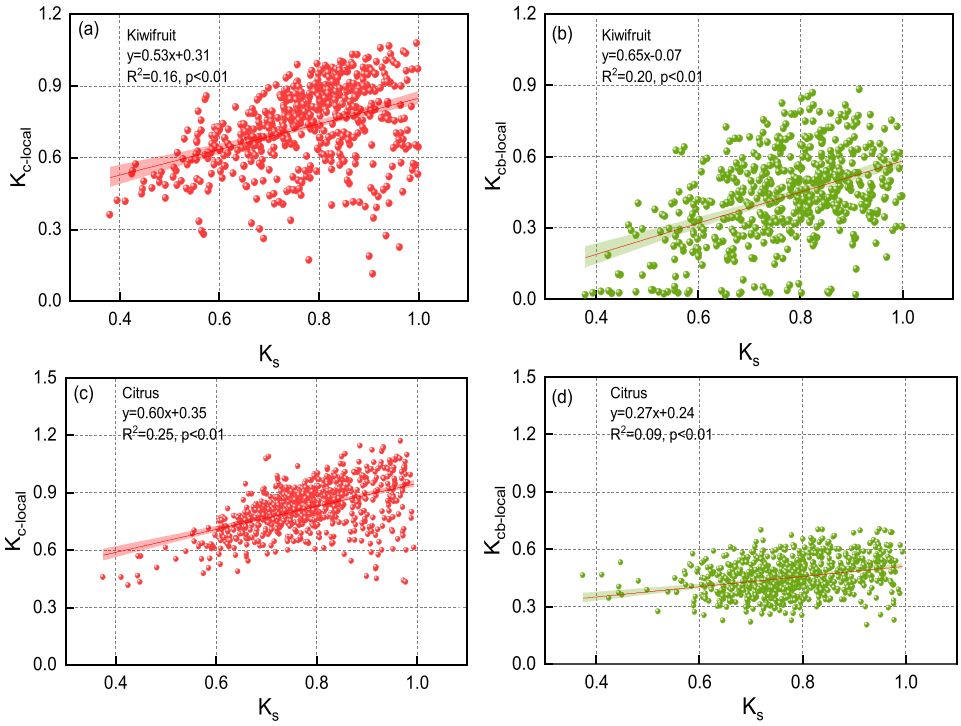

Fig. 6. The relationship between the water stress coefficient (K_s) and locally derived single crop coefficient ($K_{c\text{-local}}$) and basal crop coefficient ($K_{cb\text{-local}}$) in kiwifruit and citrus orchards.

seasonal variation trend, with values of 0.13 ± 0.02, 0.46 ± 0.05, and 0.53 ± 0.06, corresponding to the kiwifruit initial, mid-season, and late-season stages, respectively (Table 7). The $K_{cb\text{-local}}$ values of kiwifruit were consistently lower than both the $K_{c\text{-FAO56 table}}$ and $K_{c\text{-FAO56 adj}}$ values, especially during the kiwifruit mid-season and late-season stages. The standard, transferable kiwifruit stepwise K_c values ($K_{c\text{-standard}}$) were estimated at 0.74 ± 0.01, 0.99 ± 0.02 and 0.82 ± 0.01, which were slightly lower than the $K_{c\text{-FAO56 table}}$ values, while the values for K_{cb} ($K_{cb\text{-standard}}$) were estimated at 0.24 ± 0.09, 0.58 ± 0.05 and 0.63 ± 0.09 for initial, mid-season and late-season stages (Fig. 7).

Compared to kiwifruit, the $K_{c\text{-local}}$ values of citrus remained relatively stable throughout the growing season, with values of 0.72 ± 0.07, 0.85 ± 0.02 and 0.74 ± 0.08 in citrus initial, mid-season, and late-season stages (Table 8). The $K_{cb\text{-local}}$ in the citrus orchard was also relatively stable, with a value varying from 0.41 to 0.47 throughout the growing seasons, which closely matched the $K_{cb\text{-FAO56 adj}}$ (Fig. 8, Table 8). The $K_{c\text{-standard}}$ values for citrus were estimated at 0.92 ± 0.03, 1.01 ± 0.03 and 0.95 ± 0.07, which were higher than the $K_{c\text{-FAO56 table}}$, while the values for $K_{cb\text{-standard}}$ were estimated at 0.59 ± 0.03, 0.61 ± 0.02 and 0.69 ± 0.03 for citrus initial, mid-season and late-season stages.

3.5. Relationships between crop coefficient and biophysical variables

The relationships between $K_{c\text{-local}}$, $K_{cb\text{-local}}$ and LAI_t, GDD and G_s were shown in Fig. 9. Kiwifruit $K_{c\text{-local}}$ and $K_{cb\text{-local}}$ increased with an increase in LAI_t (Fig. 9a). However, citrus $K_{c\text{-local}}$ increased with increased LAI_t, and then slightly decreased when LAI_t exceeded 1.5 m^2 m^{-2} (Fig. 9b). Citrus K_{cb} decreased significantly with increased LAI_t with a linear relationship ($p < 0.01$). Both kiwifruit and citrus $K_{c\text{-local}}$ had a parabolic relationship with GDD, with peak values appearing approx. GDD of 1800 °C and 1200°C, respectively, and then decreased with an increase in GDD (Fig. 9c,d). Kiwifruit $K_{cb\text{-local}}$ increased rapidly with increased GDD, and tends to be steady when GDD exceeds 1000 °C. Contrarily, citrus $K_{cb\text{-local}}$ showed a slightly decreased trend with increasing GDD, and then increased when GDD exceeded 1000°C. The $K_{c\text{-local}}$ of kiwifruit and citrus showed a strong correlation with G_s during the growing seasons, with R^2 of 0.71 and 0.62, respectively (Fig. 9e,f). Kiwifruit $K_{cb\text{-local}}$ was also closely related to G_s during the initial and crop development stage, while no consistent relationship was found at the mid-season and late-season stages. Citrus $K_{cb\text{-local}}$ decreased rapidly with G_s, and tended to stabilize once G_s reached a certain threshold (Fig. 9f).

4. Discussion

4.1. Water use characteristics of kiwifruit and citrus orchards

The daily T in the kiwifruit orchard exhibited significant seasonal variation due to changes in canopy structure throughout the growing season, and total T/ET in kiwifruit (0.57) was higher than that of the citrus orchard (0.52) because of the higher canopy cover, though citrus was an evergreen plant. At the Qionglai station, citrus was planted with a wide row spacing configuration, which allowed light to reach the soil surface more easily and facilitated the evaporation of more soil water, resulting in a relatively lower T/ET ratio. This phenomenon of significant E contribution in widely-spaced orchards, even under drip irrigation, has also been reported in other humid and sub-humid regions (Marin and Angelocci, 2011; Zhang et al., 2011). In addition, higher E values were observed in the mid-growing season in the citrus orchards, primarily due to increased wetting events from natural precipitation, which keeps the soil surface moist and promotes E, a pattern consistent with observations in other rain-affected orchards (Ramos et al., 2023; Segovia-Cardozo, et al., 2022). However, in the kiwifruit orchard, most radiation was intercepted by the upper canopy leaves due to the horizontal canopy structure, while understory plants and soil did not receive enough energy to evaporate water, even though the soil was not suffering from water constraints during the crop mid-season stage. The seasonal dynamics of crop canopy development and meteorological variables also influence the ratio of T to ET. For instance, during the initial stages of kiwifruit, T typically constitutes a small proportion of ET, this ratio increases as the canopy develops. However, E may not decrease accordingly, owing to favorable moisture and thermal

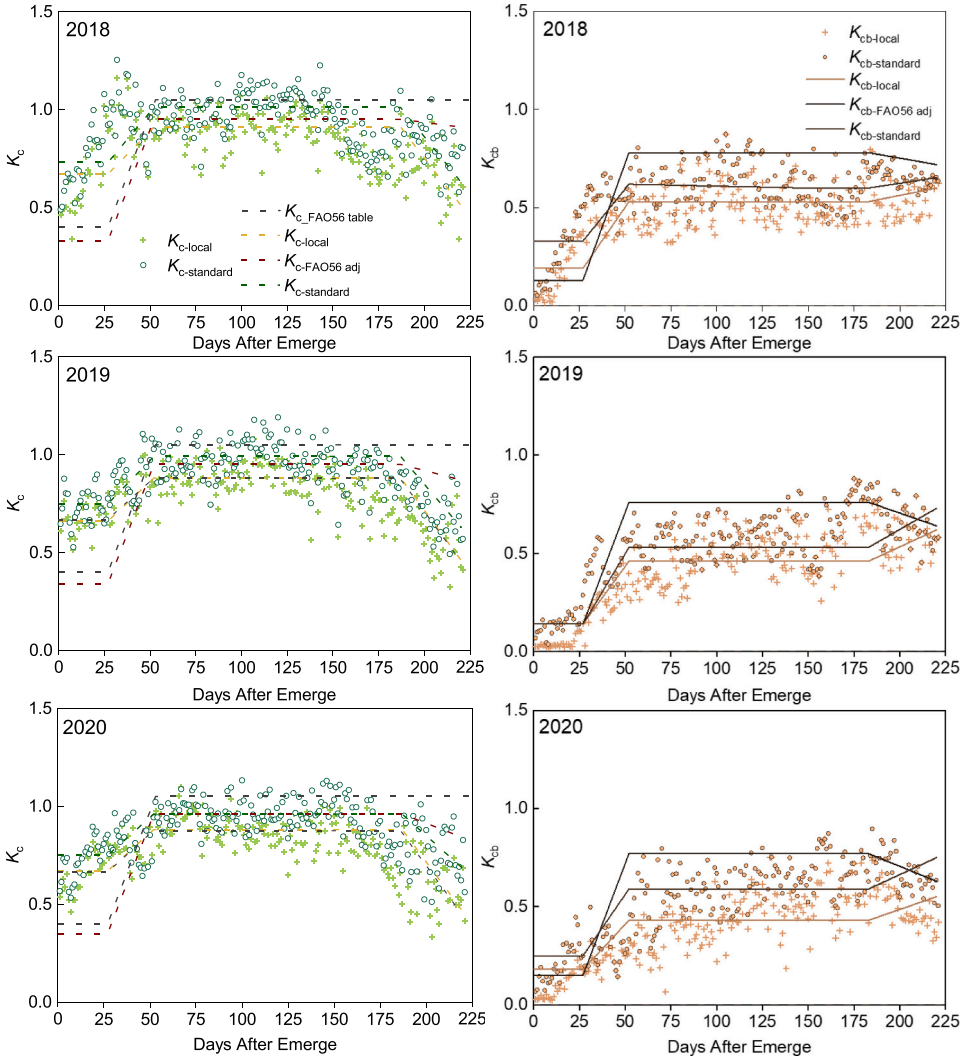

Fig. 7. Kiwifruit crop coefficients (K_c) and basal K_c (K_{cb}) derived from the observed data, the FAO-56 standard curve (the short dot line with blue), the FAO-56 adjusted curve (the dotted line with red), and the locally developed K_c and K_{cb} curves (the solid line).

conditions in midsummer. As shown in Fig. 5, *E* remained a significant component of the water flux in the kiwifruit orchard during the 2018 and 2020 growing seasons. In contrast, a noticeable reduction in *E* and *ET* occurred during midsummer of 2019, which can be attributed to decreased precipitation *P*. Meanwhile, the mature kiwifruit vines, with their deep root system, were likely still able to access soil water, sustaining a relatively high transpiration rate. This combination of suppressed *E* and sustained *T* led to *T* consistently exceeding *E* during midsummer. The observed *E* values were lower at the late-season stage in both perennial orchard sites. On the one hand, decreased seasonal rainfall reduced *E* due to soil water constraints, and on the other hand, leaves and understory vegetation gradually age in autumn, soil surface was covered by wilted grass and leaf litter cove, forming a dry matter cover layer, which increased the vapor transfer resistance of the soil surface to the atmosphere.

Kiwifruit and citrus are the top cash crops in the agricultural regions of Southwest China, with their cultivated areas rapidly expanding due to increasing market demand and rural economic development. Expanding fruit plantations in Southwest China will supplant traditional field crops, including those in the rice-wheat rotation system. Qiu et al. (2019) estimated the total *ET* for the rice-wheat rotation system in South China's humid region to be 765–841 mm/year using the Bowen ratio energy balance. The total growing season *ET* was approx.500 mm for the kiwifruit orchard, and the kiwifruit orchard was relatively bare and only weed growth occurred during the non-growing season. Therefore, the annual *ET* for the kiwifruit orchard should be less than that of the rice-wheat rotated cropland system. Besides, the total amount of citrus *ET* (600, 736 and 743 mm in 2021–2023, *ET* in the non-growing season was also included for year comparison) was also slightly less than that of the rice-wheat rotated cropland system. It seemed that the replacement of traditional field crops with fruit plantations may not be causing pressure on irrigation water resources. However, recent studies indicated that Southwest China is experiencing a warm and dry climate, leading to increased crop *ET* and heightened competition for water resources among various crops (Jiang et al.,2019a ; Wang et al., 2025). To sustain crop production in Southwest China, it is still essential to implement additional irrigation facilities and water management techniques, including water-saving irrigation engineering, agronomy, and optimization of irrigation water in Southwest China.

4.2. *Comparison of crop coefficients in different climate regions*

Accurately estimating *ET* and *T* poses a significant challenge because of variations in crop type and climatic conditions. The FAO-56 has tabulated K_c and K_{cb} values for numerous crops, however, both previously published and recently developed, may not be suitable for crops

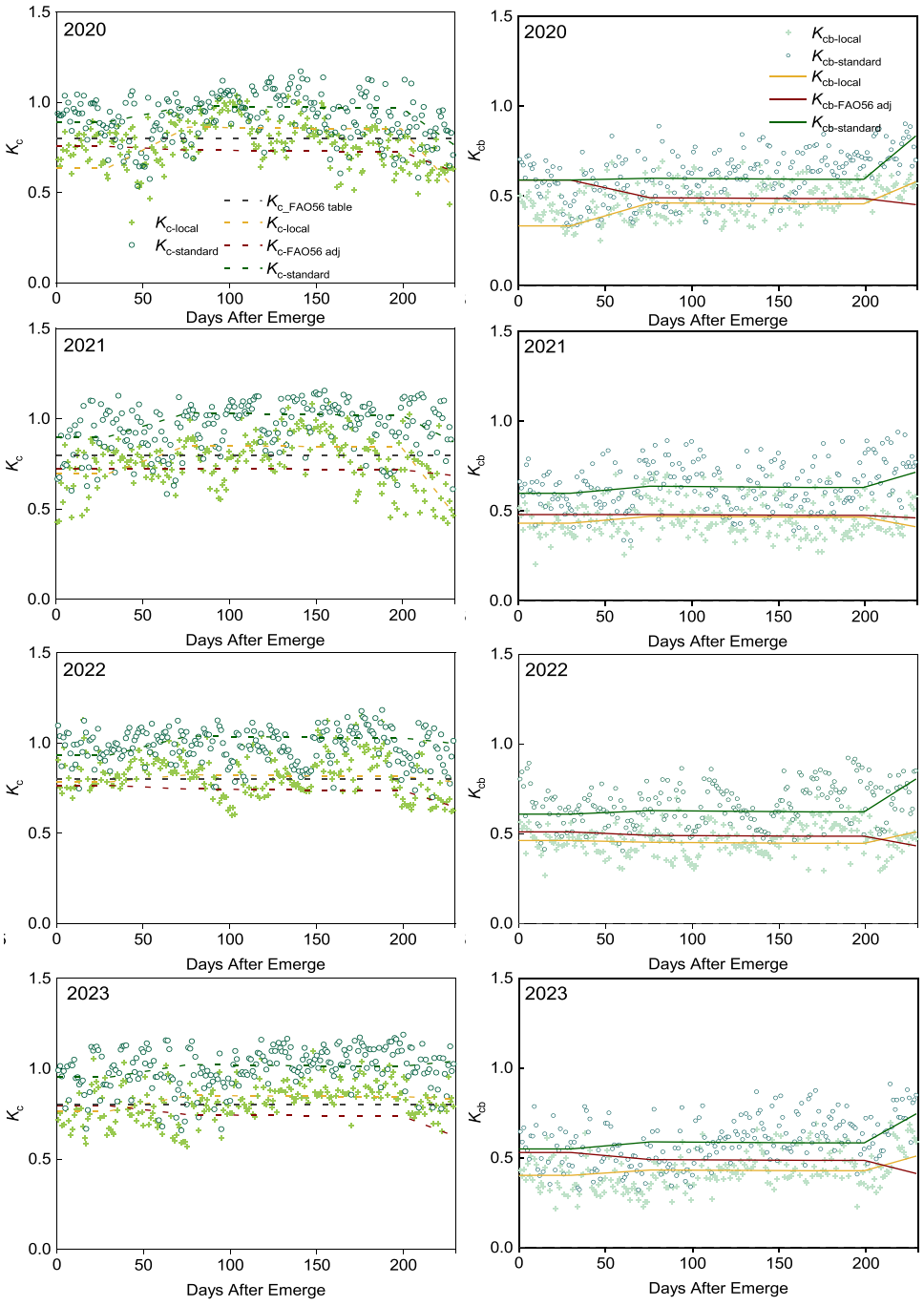

Fig. 8. Citrus crop coefficients (K_c) and basal K_c (K_{cb}) derived from the observed data, the FAO-56 standard curve (the short dot line with blue), the FAO-56 adjusted curve (the dotted line with red), and the locally developed K_c and K_{cb} curves (the solid line).

grown in different climatic regions or diverse species and plant structures, ground cover conditions and training systems, etc., (Pereira et al., 2024, López-Urrea et al., 2024). Therefore, it's essential to dynamically update standard single and basal crop coefficients for accurate crop water requirements calculation (Pereira et al., 2021 a,b).

There is a lack of reported information for kiwifruit K_c and K_{cb} in subtropical humid monsoon climates, the values derived in this study can fill this gap. This study found that the kiwifruit initial and crop development stage $K_{c\text{-standard}}$ was marginally higher than the corresponding values for generally deciduous fruit trees (apple, peach) proposed by Allen et al. (1998), such differences may stem from the larger understory *ET* during the kiwifruit initial growing season, during which weed growth occurs, and forms a green surface in the kiwifruit orchard. However, the $K_{c\text{-standard}}$ values for the kiwifruit mid-season and late-season were marginally lower than the FAO-56 tabulated K_c values in our study. It could be explained that once the kiwifruit canopy was fully developed, the expanded shaded ground led to understory vegetation growth restriction and even death, forming a dry matter mulch layer on the soil surface. This layer could prevent *E* and result in a lower K_c value (Table 7). As for the previously reported kiwifruit K_c and K_{cb}, a study conducted in a mature kiwi orchard showed that the seasonal K_c of 0.50, 1.10, and 0.80 for the kiwifruit initial, mid-season, and late-season stage, respectively (Xiloyannis et al., 2012). The reported $K_{c\text{-ini}}$ value was lower than the value derived in our study, likely because partially ground cover resulted in a lower K_c value, while the reported $K_{c\text{-mid}}$ and $K_{c\text{-end}}$ (0.99 and 0.82, respectively) were comparable to ours. Besides, a

Table 7
Comparison of the locally derived, adjusted FAO tabulated values and derived transferable standard crop coefficient (K_c) and basal K_c (K_{cb}) for the drip-irrigated kiwifruit in Southwest China.

Year	Stage	$K_{c\text{-local}}$	$K_{c\text{-FAO56 adj}}$	$K_{c\text{- standard}}$	$K_{cb\text{-local}}$	$K_{cb\text{-FAO56 adj}}$	$K_{cb\text{- standard}}$
2018	Ini	0.67	0.33	0.73	0.19	0.13	0.33
	Mid	0.91	0.95	1.01	0.53	0.78	0.62
	Lat	0.71	0.93	0.82	0.50	0.75	0.52
2019	Ini	0.66	0.34	0.75	0.14	0.14	0.14
	Mid	0.88	0.95	0.99	0.46	0.76	0.53
	Lat	0.67	0.91	0.81	0.60	0.70	0.68
2020	Ini	0.68	0.35	0.75	0.18	0.15	0.25
	Mid	0.88	0.96	0.96	0.43	0.77	0.59
	Lat	0.67	0.90	0.82	0.49	0.70	0.67
Average	Ini	0.67 ± 0.01	0.34 ± 0.01	0.74 ± 0.01	0.13 ± 0.02	0.14 ± 0.01	0.24 ± 0.09
	Mid	0.89 ± 0.02	0.95 ± 0.01	0.99 ± 0.02	0.46 ± 0.05	0.77 ± 0.01	0.58 ± 0.05
	Lat	0.68 ± 0.02	0.91 ± 0.02	0.82 ± 0.01	0.53 ± 0.06	0.71 ± 0.03	0.63 ± 0.09

Table 8
Comparison of the locally derived, adjusted and derived transferable standard crop coefficient (K_c) and basal K_c (K_{cb}) for the drip-irrigated citrus in Southwest China.

Year	Stage	$K_{c\text{-local}}$	$K_{c\text{-FAO56 adj}}$	$K_{c\text{-standard}}$	$K_{cb\text{-local}}$	$K_{cb\text{-FAO56 adj}}$	$K_{cb\text{- standard}}$
2020	Ini	0.65	0.77	0.91	0.34	0.60	0.60
	Mid	0.88	0.75	1.00	0.47	0.50	0.61
	Lat	0.71	0.69	0.89	0.53	0.48	0.73
2021	Ini	0.71	0.74	0.92	0.44	0.49	0.61
	Mid	0.87	0.74	1.05	0.48	0.49	0.65
	Lat	0.68	0.72	0.97	0.45	0.48	0.69
2022	Ini	0.80	0.78	0.95	0.47	0.52	0.62
	Mid	0.84	0.76	1.06	0.46	0.50	0.64
	Lat	0.82	0.71	1.01	0.49	0.47	0.73
2023	Ini	0.78	0.81	0.97	0.41	0.54	0.56
	Mid	0.87	0.76	1.04	0.44	500.50	0.60
	Lat	0.85	0.70	1.05	0.48	0.46	0.68
Average	Ini	0.72 ± 0.07	0.76 ± 0.03	0.92 ± 0.03	0.41 ± 0.05	0.53 ± 0.05	0.59 ± 0.03
	Mid	0.85 ± 0.02	0.74 ± 0.01	1.01 ± 0.03	0.45 ± 0.02	0.49 ± 0.01	0.61 ± 0.02
	Lat	0.74 ± 0.08	0.68 ± 0.01	0.95 ± 0.07	0.47 ± 0.03	0.46 ± 0.01	0.69 ± 0.03

similar kiwifruit mid-season K_c value was reported as 0.95 by Silva et al. (2008) in the Mediterranean climate. The slight difference between K_c or K_{cb} across the different observed sites was allowed due to different climate characteristics and plant conditions, i.e., ground cover, training system, etc., as concluded by López-Urrea et al. (2024).

The citrus $K_{c\text{-local}}$ values were comparable to most reports conducted in different climate regions, while staged $K_{c\text{-standard}}$ values were generally higher than $K_{c\text{-FAO56 table}}$ values. Besides, $K_{c\text{-standard}}$ numbers exceed $K_{c\text{-derived}}$ by substantial amounts. In this study, citrus was planted in subtropical humid monsoon climates, with the observed annual average u_2 and RH_{min} being 0.87 m s^{-1} and 62.7 %, respectively. Therefore, higher air relative humidity and lower wind speed may be the reason causing substantial deviation between $K_{c\text{-standard}}$ and $K_{c\text{-derived}}$ (Eq. 21), highlighting the importance of atmosphere correction for crop coefficients, especially in such climatic regions (Rogers et al.,1983). In addition, a seasonal citrus K_c was found throughout the growing seasons. As concluded by Peddinti and Kambhammettu (2019), seasonal citrus K_c values were 0.80 ± 0.22 (initial), 0.87 ± 0.14 (mid), and 0.91 ± 0.13 (late) in tropical to dry climates of the USA, whereas the values were 0.55 ± 0.24, 0.51 ± 0.18, and 0.62 ± 0.12, respectively, in tropical to temperate climates of Brazil, and 0.39 ± 0.13, 0.87 ± 0.17, and 0.91 ± 0.09, in Mediterranean climates in Spain. The lower K_c values in the tropical climate of Brazil were due to citrus leaves restricting water loss under high atmospheric water demand (Marin and Angelocci, 2011). Seasonal $K_{c\text{-standard}}$ for citrus obtained in this study aligned with those documented for tropical to dry climates in the USA, with mid- and late-season values consistent with the upper observations in Mediterranean climates. A review of locally developed K_c and K_{cb} values for citrus across various climate types in other regions is presented in Table 9. Citrus, being an evergreen tree, typically has constant K_c values throughout the growing season as recommended in FAO-56. While some studies showed a K_c curve, with higher values at the crop initial and late-season stage, particularly in Mediterranean climates characterized by minimal summer precipitation (mid-season stage, Table 9) (Maestre-Valero et al., 2017; Segovia-Cardozo et al., 2022; Ramos et al., 2023). Seasonal K_c was also found in our study, with higher K_c values occurring during the mid-season stage, during which abundant precipitation occurred, affected by the monsoon climate, which contrasts with the FAO reports (Section 4.3 for the reason). Therefore, using a constant K_c may not be appropriate for citrus cultivated with wide rows when they undergo seasonal precipitation during the growing season.

Seasonal K_{cb} values for citrus trees have been observed across diverse climates (Taylor, 2015; Segovia-Cardozo et al., 2022; Jafari et al., 2021). The derived citrus staged K_{cb} values in our study were within the reported range, and the higher $K_{cb\text{-end}}$ value may be due to soil-to-canopy advection enhancing T at the citrus late-season stages. Er-Raki et al. (2009) indicated that the three-staged K_{cb} values for citrus orchards in Morocco were 0.3, 0.5, and 0.4 under flood irrigation and 0.35, 0.55, and 0.45 under drip irrigation management. Alves et al. (2007) demonstrated that K_{cb} values for young lime orchards ranged from 0.4 to 1.0 throughout the growing season in the tropical and temperate climates of Brazil. Taylor et al. (2015) calibrated K_{cb} for citrus, varying from 0.35 to 0.43, using the heat ratio method. Totally, various studies have also reported that the stagewise K_{cb} varied from 0.34 to 0.63, 0.37–0.72, 0.38–0.90 in citrus initial, mid-season and late-season stages, respectively (Pereira et al., 2024). The staged $K_{cb\text{-standard}}$ in this study was within the reported range, but the late-season stage $K_{cb\text{-standard}}$ (0.68–0.73) was slightly higher than that in most reports and the initial and mid-season $K_{cb\text{-standard}}$ reported in our study (Taylor et al., 2015; Maestre-Valero et al., 2017; Ramos et al., 2023). Decreased precipitation during the citrus late-season stage caused a relatively dry condition within the row, since citrus root soil water can be supplied using a drip irrigation system, and within-field advection existed between the crop canopy and row soil. The transfer of hot air from a warmer to a cooler

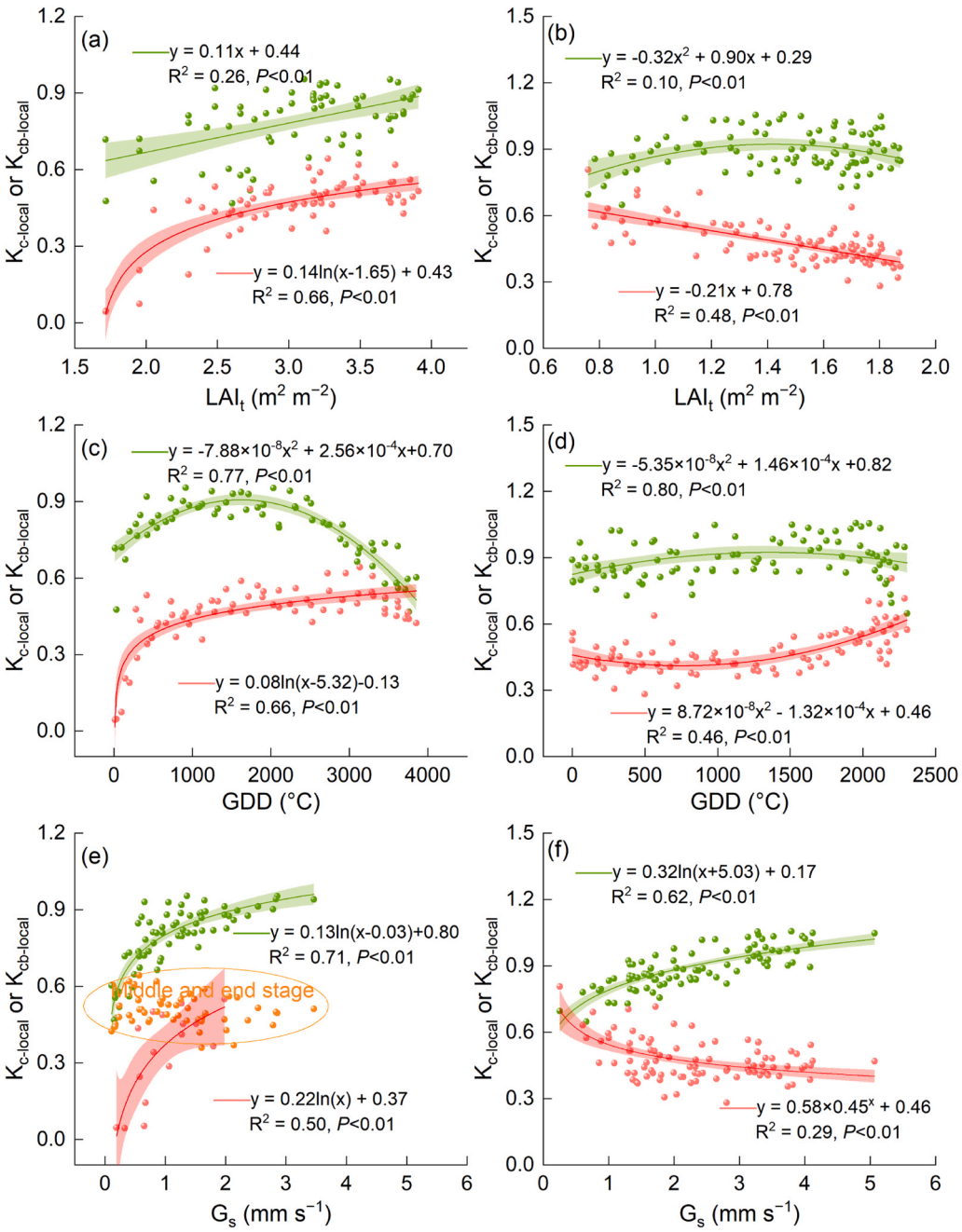

Fig. 9. The relationship between the 10-moving averages of local derived crop coefficient ($K_{c\text{-local}}$), basal crop coefficient ($K_{cb\text{-local}}$) and total leaf area index (LAI_t), Growing degree days (GDD) and underlying conductance (G_s) in the kiwifruit (Left) and citrus orchard (Right).

surface can increase evaporation by supplying additional energy, provided that water is accessible (Kool et al., 2018). Therefore, soil-to-canopy advection may enhance T at the citrus late-season stage, which causes a higher $K_{cb\text{-standard}}$ (Allen et al., 2011).

4.3. Seasonal variation of underlying conditions affecting crop coefficient

The crop coefficient method is widely recognized for estimating ET and T, with numerous studies confirming that single and dual crop coefficient methods effectively evaluate daily ET and its components with the calibrated coefficient by the measured value at various growth stages (Anapalli et al., 2020; Liu et al., 2023; Zhang et al., 2023). However, actual K_c and K_{cb} are affected by local climate conditions, vegetation and water availability (Segovia-Cardozo et al., 2022). For instance, the occurrence of $K_s < 1$ during the initial and late-season stage partly explains the lower $K_{c\text{-local}}$ and $K_{cb\text{-local}}$ values in both kiwifruit and citrus orchard, as soil moisture deficits reduced actual ET and T (Fig. 6).

Several researchers have demonstrated a strong correlation between K_c and crop leaf area (Pereira et al., 2021a; Wang et al., 2023), canopy cover (Carpintero et al., 2020), and the fraction of light intercepted by the canopy (Williams and Ayars, 2005), with linear or polynomial characteristics. Therefore, the K_c and K_{cb} values in kiwifruit croplands varied seasonally due to the seasonal changes in LAI and canopy cover, which is a typical pattern in such deciduous broadleaf orchards. As a reflection of crop phenology, GDD also exhibited a polynomial relationship with K_c and K_{cb} in kiwifruit and citrus orchards, aligning with previous studies (Ji et al., 2017; Guo et al., 2020). Although the LAI_t reflects the overall regulation of the vegetation community on water flux, the relationship between LAI_t and K_c or K_{cb}, as well as its functional form, can vary significantly owing to the dynamics of crop physiological

Table 9
Comparison of locally developed crop coefficients (K_c) for the citrus crops in other regions under different climates.

Author	Location and main climate	*ET* measurements (ET_o equation)	Irrigation method and strategy	f_c or f_{IPAR}	Age (years)	Height	Ground cover	Derived averaged staged K_c	Derived staged K_{cb}
Maestre-Valero et al. (2017)	Valencia, Spain Med. Semi-arid	EC (FAO-PM-ET_o)	Drip FI	0.66	mature	2.8	BS	1.11 , 0.74 and 0.99	0.63, 0.53 and 0.58
Segovia-Card ozo et al. (2022)	Palermo, ltaly Med. dry	SF, SWB-FDR(FAO-PM-ET_o)	Micro-spr, Drip and FI	0.40	30	2.5	AGC Aut-Spr	0.95, 0.43 and 0.95	n/r, 0.39 and 0.90
lppolito et al. (2023)	Palermo, Italy Med., dry	EC, SWB-FDR, Kc-VI (FAO-PM-ET_o)	Drip DI	0.50	mature	2.5	AGC	n/r, 0.55 and 0.75	n/r
Ramos et al., (2023)	Aljustrel, Portugal Med., dry	SWB-TDR SIMDualKc (FAO-PM-ET_o)	Drip and FI	0.29	5–6	2.8	AGC Aut-Spr	0.94, 0.50 and 0.93	0.40, 0.40 and 0.40
Peddinti and Kambhammettu (2019)	Vidabha, central India	EC, SF, SWB-ML, SIMDualKc (FAO-PM-ET_o)	Flood, Drip and deficit irrigation	0.70	8	2.5–3.0	BS	0.80, 0.65 and 0.80	0.60, 0.45 and 0.55
Jafari et al. (2021)	Fars, Southern Iran Semi-arid	SWB-neutron, ML (FAO-PM-ET_o)	Drip and FI	0.85	25	3.0	BS	0.68, 0.87 and 0.81	0.59, 0.72 and 0.72
Jia et al. (2007)	Central Florida Sub-tropical humid	EC (ASCE-PM-ET_o)	Micro-spr	n/r	16	4.5–5.5	BS	0.73,0.93 and 1.07	n/r
Castel (2000)	Valencia, Spain Med. Semi-arid	WL (FAO-PM-ET_o)	Drip and FI	0.09–0.38	6–14	1.7–2.3	AGC	0.33–0.75,0.30–0.55,0.38–0.66	n/r
Taylor et al. (2015)	Limpopo, S. Africa Summer rainfall	SF, A&P app (FAO-PM-ET_o)	Drip and FI	0.60	11	4.1	BS	n/r	0.40, 0.41 and 0.42
Taylor et al. (2015)	Limpopo, S. Africa Summer rainfall	SF, A&P app (FAO-PM-ET_o)	Drip and FI	0.63	6	2.3	BS	n/r	0.34, 0.37 and 0.38
Taylor et al. (2015, 2017)	Western Cape, RSA Winter rainfall	SF, A&P app (FAO-PM-ET_o)	Drip and FI	0.88	14	3.3	BS	n/r	0.50, 0.35 and 0.80

Note: Ly is lysimeters, EC is the eddy covariance technique, BREB is the Bowen-ratio energy balance system, WB is the Water balance method, SF is the sap flow technique. WL is weighing lysimeter, A&P represents the Allen and Pereira (2009) approach, AGC and BS represent the active ground cover and bare soil characteristics. FDR and TDR represent the frequency domain reflectometer and time domain reflectometer, respectively. FI is the full irrigation, Micro-spr is Micro-sprinkler or micro-sprayer. FAO-PM-ET_o is the grass reference, ET_o represents the values computed with full data.

regulation and the underlying crop characteristics (Segovia-Cardozo et al., 2022). For instance, a negative relationship was found between LAI_t and K_{cb} in citrus orchard, and the possible reason was that the increased T_a and *VPD* during the summertime caused a stomatal limitation for citrus leaves, which constrained the canopy transpiration and resulted in a lower K_{cb} value, though the active ground cover increased (Segovia-Cardozo et al., 2022). G_s combines the physical and physiological variations between the crop-specific and reference surfaces, and is expected to describe the dynamics of the K_c and K_{cb} (Wang et al., 2023). Good logarithmic relationships were observed between K_c and G_s in our study, and K_c increased with G_s and tended to stabilize once G_s reached a certain threshold (Fig. 9), aligning with findings from Wang et al., (2020). Previous studies have found that competition among individual leaves for radiation was increased under higher *LAI* or canopy coverage, which decreased *T* per unit of leaf area. Therefore, K_c and K_{cb} tended to remain stable when *LAI* or G_s were higher.

Both local actual and standard K_c and K_{cb} values for citrus in our study and other studies showed seasonal variations, contradicting the constant value recommended by FAO-56 (Jafari et al., 2021; Jamshidi et al., 2020; Peddinti and Kambhammettu, 2019). Citrus is commonly planted sparsely in wide rows, a common practice in Southwest China. Seasonally drying, caused by decreased precipitation, occurs annually during the citrus's initial and late-season stages, limiting *E* within the row. This resulted in a lower $K_{c\text{-}ini}$ despite the drip irrigation being applied to supply water for the crops. During the wet period, the frequency of rainfall events and increased soil moisture facilitated the active growth of ground cover within the row, leading to elevated K_c values during the mid-season stage (Kool et al., 2018; Qin et al., 2023). As the growing season progressed, soil moisture storage was depleted due to limited rainfall. The surface was inadequately watered and the soil was completely covered by dry weeds, which inhibited soil surface evaporation (Petry et al., 2024). Therefore, decreased K_c values have been observed during the late-season stage of citrus orchards (Segovia-Cardozo et al., 2022). The increased K_{cb} during the late-season stage confirmed the changes in soil water content attributed exclusively to the citrus *T* process, since citrus root soil water can be supplied using a drip irrigation system, and a dry environment may also enhance citrus *T* (Pereira et al., 2020; Nandi et al., 2023; Qin et al., 2023). This outcome was anticipated as the K_c values closely matched the corresponding K_{cb} when *ET* was primarily influenced by tree *T*, with minimal ground transpiration in the late-season stage.

While this study provides robust locally calibrated crop coefficients, it is important to acknowledge certain limitations. The estimation of ET_o using the FAO-56 Penman-Monteith equation was conducted within the orchard environment, which differs from the standard well-watered grass reference surface. This approach, though practical and widely adopted in the absence of an ideal reference site, may introduce biases due to the altered aerodynamic and surface resistance characteristics of the orchard. Future research should explore the development of ET_o correction frameworks or alternative reference surfaces that better represent the microclimatic conditions of perennial cropping systems in humid regions.

5. Conclusion

Based on the two EC experimental sites conducted in orchard sites (kiwifruit and citrus), this study provided a comprehensive analysis of energy partitioning, water use dynamics, and crop coefficients for the two represented orchard agroecosystems in the humid subtropical region of Southwest China. The energy flux components and *ET* exhibited notable seasonal variability, with R_n predominantly consumed as *LE* during the entire growing season. Daily average *ET* was 2.04 ± 0.18 mm d^{-1} for kiwifruit and 2.49 ± 0.25 mm d^{-1} for citrus, with *T* contributing over 50 % of the total *ET* in both orchards. The derived $K_{c\text{-standard}}$ for kiwifruit was 0.74 ± 0.01 at the initial stage ($K_{c\text{-ini}}$), 0.99 ± 0.02 at the mid-season stage ($K_{c\text{-mid}}$), and 0.82 ± 0.01 at the late-season stage ($K_{c\text{-end}}$), while the stagewise value for $K_{cb\text{-standard}}$ was 0.24 ± 0.09, 0.58 ± 0.05 and 0.63 ± 0.09. For citrus, the corresponding $K_{c\text{-ini}}$, $K_{c\text{-mid}}$ and $K_{c\text{-end}}$ were derived at 0.92 ± 0.03, 1.01 ± 0.03 and 0.95 ± 0.07, while the stagewise $K_{cb\text{-standard}}$ values were 0.59 ± 0.03, 0.61 ± 0.02 and 0.69 ± 0.03, respectively. Both $K_{c\text{-local}}$ and $K_{cb\text{-local}}$ were significantly regulated by biophysical variables (including *LAI*, *GDD* and G_s). Seasonal precipitation patterns and active ground cover in orchard rows affected $K_{c\text{-local}}$ and $K_{cb\text{-local}}$, especially for citrus orchards planted with wide rows, highlighting the limitations of applying FAO-56 tabulated values directly in humid subtropical orchards with active ground cover and wide row spacing. This study provides the long-term, dual-crop coefficient dataset for kiwifruit and citrus in this region, offering practical tools for improving water management in similar agroecosystems. Future work should focus on developing dynamic K_c models that integrate vegetation indices and soil moisture data to support precision irrigation.

CRediT authorship contribution statement

Chenggaoge Yang: Validation, Resources, Conceptualization. **Ningbo Cui:** Validation, Resources, Data curation, Conceptualization. **Shouzheng Jiang:** Writing – review & editing, Writing – original draft, Visualization, Validation, Software, Resources, Methodology, Investigation, Data curation, Conceptualization. **Jingyuan Xue:** Validation, Resources, Data curation, Conceptualization. **Zhihui Wang:** Writing – review & editing, Validation, Software, Methodology, Data curation, Conceptualization. **Lu Zhao:** Validation, Resources, Conceptualization. **Xiaoxian Zhang:** Writing – review & editing, Methodology, Conceptualization. **Yu Feng:** Validation, Resources, Conceptualization. **Daozhi Gong:** Validation, Resources, Conceptualization, Methodology, Supervision, Writing – review & editing. **Xiuyun Yu:** Conceptualization, Data curation, Resources, Validation, Investigation, Methodology, Software, Visualization, Writing – original draft.

Declaration of Competing Interest

The authors declare that they have no known competing financial interests or personal relationships that could have appeared to influence the work reported in this paper.

Acknowledgment

This work was also financially funded by the National Key Research and Development Program of China (2023YFD1901203, 2021YFD1600803-1), National Natural Science Foundation of China (52309055, 52279041), Sichuan Province Science and Technology Program (2023YFN0024), Fundamental Research Funds for the Central Universities (YJ202259), Training Program of the Innovation Guidance and Scientific and Technological Enterprise of Yunnan Province (202304BT090019), and the Technological Innovation and R&D Project of Chengdu Eastern New Area (2024-DBXQ-KJYF008-LH). Thanks to the anonymous reviewers and editors for their comments, which has helped improve the quality of this text. The birth of little Jiang has always inspired me to continuously improve the quality of this text.

Appendix A. Supporting information

Supplementary data associated with this article can be found in the online version at doi:10.1016/j.agwat.2025.109984.

Data availability

Data will be made available on request.

References

Allen, R.G., Pereira, L.S., Howell, T.A., Jensen, M.E., 2011. Evapotranspiration information reporting: I. Factors governing measurement accuracy. Agric. Water Manag. 98 (6), 899–920.
Allen, R.G., Pereira, L.S., Raes, D., Smith, M., 1998. Crop evapotranspiration- guidelines for computing crop water requirements, irrigation and drain, Paper No, 56. FAO, Rome, Italy, p. 300.
Allen, R.G., Pereira, L.S., 2009. Estimating crop coefficients from fraction of ground cover and height. Irrig Sci 28, 17–34.
Alves, J., Folegatti, M.V., Parsons, L.R., Bandaranayake, W., da Silva, C.R., da Silva, T.J. A., Campeche, L.F.S.M., 2007. Determination of the crop coefficient for grafted 'Tahiti' lime trees and soil evaporation coefficient of Rhodic Kandiudalf clay soil in Sao Paulo, Brazil. Irrig. Sci. 25, 419–428.
Anapalli, S.S., Fisher, D.K., Pinnamaneni, S.R., Reddy, K.N., 2020. Quantifying evapotranspiration and crop coefficients for cotton (*Gossypium hirsutum* L.) using an eddy covariance approach. Agric. Water Manag 233, 106091.
Anderson, R.G., Alfieri, J.G., Tirado-Corbalá, R., Gartung, J., McKee, L.G., Prueger, J.H., Wang, D., Ayars, J.E., Kustas, W.P., 2017. Assessing FAO-56 dual crop coefficients using eddy covariance flux partitioning. Agric. Water Manag 179, 92–102.
ASCE-EWRI, 2005. The ASCE standardized reference evapotranspiration equation. Report 0-7844-0805-X, ASCE task committee on standardization of reference evapotranspiration. American Soc. Civil Engineers, Reston, Va.
Bian, J., Hu, X., Shi, L., Min, L., Zhang, Y., Shen, Y., Zhao, F., Zha, Y., Lian, X., Huang, J., 2024. Evapotranspiration partitioning by integrating eddy covariance, micro-lysimeter and unmanned aerial vehicle observations: A case study in the North China Plain. Agric. Water Manag 295, 108735.
Burchard-Levine, V., Nieto, H., Riano, D., Kustas, W.P., Migliavacca, M., El-Madany, T.S., Nelson, J.A., Andreu, A., Carrara, A., Beringer, J., Baldocchi, D., Martin, M.P., 2022. A remote sensing-based three-source energy balance model to improve global estimations of evapotranspiration in semi-arid tree-grass ecosystems. Glob. Change Biol. 28, 1493–1515.
Carpintero, E., Mateos, L., Andreu, A., González-Dugo, M.P., 2020. Effect of the differences in spectral response of Mediterranean tree canopies on the estimation of evapotranspiration using vegetation index-based crop coefficients. Agric. Water Manag 238, 106201.
Castel, J.R., 2000. Water use of developing citrus canopies in Valencia, Spain. In: In: Proc Int Soc Citriculture. IX Congr Florida, USA, pp. 223–226.
Chen, F., Cui, N., Jiang, S., Wang, Z., Li, H., Lv, M., Wang, Y., Gong, D., Zhao, L., 2023. Multi-objective deficit drip irrigation optimization of citrus yield, fruit quality and water use efficiency using NSGA-II in seasonal arid area of Southwest China. Agric. Water Manag 287, 108440.
Cui, W., Chui, T.F.M., 2019. Temporal and spatial variations of energy balance closure across FLUXNET research sites. Agric. For. Meteor. 271, 12–21.
Cui, N., He, Z., Jiang, S., Wang, M., Yu, X., Zhao, L., Qiu, R., Gong, D., Wang, Y., Feng, Y., 2023. Inter-comparison of the Penman-Monteith type model in modeling the evapotranspiration and its components in an orchard plantation of Southwest China. Agric. Water Manag 289, 108541.
Er-Raki, S., Chehbouni, A., Guemouria, N., Ezzahar, J., Khabba, S., Boulet, G., Hanich, L., 2009. Citrus orchard evapotranspiration: comparison between eddy covariance measurements and the FAO-56 approach estimates. Plant Biosyst. 143, 201–208.
Ershadi, A., McCabe, M.F., Evans, J.P., Wood, E.F., 2015. Impact of model structure and parameterization on Penman–Monteith type evaporation models. J. Hydrol. 525, 521–535.
Falge, E., Baldocchi, D., Olson, R., Anthoni, P., Aubinet, M., Bernhofer, C., Burba, G., Ceulemans, R., Clement, R., Dolman, H., Granier, A., Gross, P., Grunwald, T., Hollinger, D., Jensen, N.O., Katul, G., Keronen, P., Kowalski, A., Lai, C.T., Law, B.E., Meyers, T., Moncrieff, H., Moors, E., Munger, J.W., Pilegaard, K., Rannik, U., Rebmann, C., Suyker, A., Tenhunen, J., Tu, K., Verma, S., Vesala, T., Wilson, K., Wofsy, S., 2001. Gap filling strategies for defensible annual sums of net ecosystem exchange. Agric. For. Meteor. 107, 43–69.
Flo, V., Martinez-Vilalta, J., Steppe, K., Schuldt, B., Poyatos, R., 2019. A synthesis of bias and uncertainty in sap flow methods. Agric. For. Meteor. 271, 362–374.
Gan, G., Liu, Y., 2020. Inferring transpiration from evapotranspiration: a transpiration indicator using the Priestley-Taylor coefficient of wet environment. Ecol. Indic. 110, 105853.
Gebler, S., Franssen, H.J.H., Puetz, T., Post, H., Schmidt, M., Vereecken, H., 2015. Actual evapotranspiration and precipitation measured by lysimeters: a comparison with eddy covariance and tipping bucket. Hydrol. Earth Syst. Sci. 19, 2145–2161.

Gong, X., Liu, H., Sun, J., Gao, Y., Zhang, H., 2019. Comparison of Shuttleworth-Wallace model and dual crop coefficient method for estimating evapotranspiration of tomato cultivated in a solar greenhouse. Agric. Water Manag 217, 141–153.
Gong, D., Mei, X., Hao, W., Wang, H., Caylor, K.K., 2017. Comparison of ET partitioning and crop coefficients between partial plastic mulched and non-mulched maize fields. Agric. Water Manag 181, 23–34.
Gong, X., Qiu, R., Sun, J., Ge, J., Li, Y., Wang, S., 2020. Evapotranspiration and crop coefficient of tomato grown in a solar greenhouse under full and deficit irrigation. Agric. Water Manag. 235, 106154.
Granier, A., 1987. Evaluation of transpiration in a douglas-fir stand by means of sap flow measurements. Tree Physiol. 3 (4), 309–319.
Guo, H., Li, S., Kang, S., Du, T., Tong, L., Hao, X., Ding, R., 2020. Crop coefficient for spring maize under plastic mulch based on 12-year eddy covariance observation in the arid region of Northwest China. J. Hydrol. 588, 125108.
Huang, L., Lin, X., Jiang, S., Liu, M., Jiang, Y., Li, Z.-L., Tang, R., 2022. A two-stage light-use efficiency model for improving gross primary production estimation in agroecosystems. Environ. Res. Lett. 17, 104021.
Jafari, M., Kamali, H., Keshavarz, A., Momeni, A., 2021. Estimation of evapotranspiration and crop coefficient of drip-irrigated orange trees under a semi-arid climate. Agric. Water Manag 248, 106769.
Jamshidi, S., Zand-Parsa, S., Kamgar-Haghighi, A.A., Shahsavar, A.R., Niyogi, D., 2020. Evapotranspiration, crop coefficients, and physiological responses of citrus trees in semi-arid climatic conditions. Agric. Water Manag 227, 105838.
Ji, X.B., Chen, J.M., Zhao, W.Z., Kang, E.S., Jin, B.W., Xu, S.Q., 2017. Comparison of hourly and daily Penman-Monteith grass- and alfalfa-reference evapotranspiration equations and crop coefficients for maize under arid climatic conditions. Agric. Water Manag. 192, 1–11.
Jia, X., Swancar, A., Jacobs, J.M., Dukes, M.D., Morgan, K., 2007. Comparison of evapotranspiration rates for flatwoods and ridge citrus. Trans ASABE 50 (1), 83–94.
Jiang, X., Kang, S., Tong, L., Li, S., Ding, R., Du, T., 2019b. Modeling evapotranspiration and its components of maize for seed production in an arid region of northwest China using a dual crop coefficient and multisource models. Agric. Water Manag 222, 105–117.
Jiang, S., Liang, C., Cui, N., Zhao, L., Du, T., Hu, X., Feng, Y., Guan, J., Feng, Y., 2019a. Impacts of climatic variables on reference evapotranspiration during growing season in Southwest China. Agric. Water Manag 216, 365–378.
Jiang, S., Liang, C., Zhao, L., Gong, D., Huang, Y., Xing, L., Zhu, S., Feng, Y., Guo, L., Cui, N., 2022a. Energy and evapotranspiration partitioning over a humid region orchard: Field measurements and partitioning model comparisons. J. Hydrol. 610, 127890.
Jiang, S., Zhao, L., Liang, C., Hu, X., Wang, Y., Gong, D., Zheng, S., Huang, Y., He, Q., Cui, N., 2022b. Leaf- and ecosystem-scale water use efficiency and their controlling factors of a kiwifruit orchard in the humid region of Southwest China. Agric. Water Manag 260, 107329.
Jonsson, P., Eklundh, L., 2004. TIMESAT - a program for analyzing time-series of satellite sensor data. Comput. Geosci. 30, 833–845.
Kalfas, J.L., Xiao, X., Vanegas, D.X., Verma, S.B., Suyker, A.E., 2011. Modeling gross primary production of irrigated and rain-fed maize using MODIS imagery and CO_2 flux tower data. Agric. For. Meteor. 151, 1514–1528.
Kato, T., Kamichika, M., 2006. Determination of a crop coefficient for evapotranspiration in a sparse sorghum field. Irrig. Drain. 55, 165–175.
Kool, D., Ben-Gal, A., Agam, N., 2018. Within-field advection enhances evaporation and transpiration in a vineyard in an arid environment. Agric. For. Meteor. 255, 104–113.
Kwon, S.H., Yun, S.K., Kim, S.S., Park, Y., 2021. Phenological shifts of buds and flowers caused by early heat recognition in citrus in Jeju, Korea. Sci. Hortic. 283, 110092..
Liu, B., Hou, J., Ge, H., Liu, M., Shi, L., Li, C., Cui, Y., 2023. Comparison of evapotranspiration partitioning and dual crop coefficients of Direct-Seeded and transplanted rice in the Poyang lake basin, China. Agron. Basel 13 (5), 1218.
López-Urrea, R., Oliveira, C.M., Montoya, F., Paredes, P., Pereira, L.S., 2024. Single and basal crop coefficients for temperate climate fruit trees, vines and shrubs with consideration of fraction of ground cover, height, and training system. Irrig. Sci. 42, 1099–1135.
Maestre-Valero, J.F., Testi, L., Jiménez-Bello, M.A., Castel, J.R., Intrigliolo, D.S., 2017. Evapotranspiration and carbon exchange in a citrus orchard using eddy covariance. Irrig. Sci. 35, 397–408.
Marin, F.R., Angelocci, L.R., 2011. Irrigation requirements and transpiration coupling to the atmosphere of a citrus orchard in Southern Brazil. Agric. Water Manag. 98, 1091–1096.
Mebrie, D.W., Assefa, T.T., Yimam, A.Y., Belay, S.A., 2023. A remote sensing approach to estimate variable crop coefficient and evapotranspiration for improved water productivity in the Ethiopian highlands. Appl. Water Sci. 13, 168.
Mobe, N.T., Dzikiti, S., Zirebwa, S.F., Midgley, S.J.E., von Loeper, W., Mazvimavi, D., Ntshidi, Z., Jovanovic, N.Z., 2020. Estimating crop coefficients for apple orchards with varying canopy cover using measured data from twelve orchards in the Western Cape Province, South Africa. Agric. Water Manag 233, 106103.
Molina, A., Aranda, J., Carta, X., Llorens, G., Romero, P., Savé, R., Biel, C, R., 2016. Effect of irrigation on sap flux density variability and water use estimate in cherry (*Prunus avium*) for timber production: Azimuthal profile, radial profile and sapwood estimation. Agric. Water Manag 164, 118–126.
Monteith, J.L., 1965. Evaporation and environment. Symp. Soc. Exp. Biol. 19, 205–234.
Nandi, R., Mudi, D.K., Singh, K.C., Saha, M., Bandyopadhyay, P.K., 2023. Partitioning of evapotranspiration and crop coefficients of lentil under conserved soil moisture conditions. J. Soil Sci. Plant Nutr. 24, 435–450.
Peddinti, S.R., Kambhammettu, B.P., 2019. Dynamics of crop coefficients for citrus orchards of central India using water balance and eddy covariance flux partition techniques. Agric. Water Manag 212, 68–77.
Pereira, L.S., Paredes, P., Hunsaker, D.J., López-Urrea, R., Mohammadi Shad, Z., 2021a. Standard single and basal crop coefficients for field crops. Updates and advances to the FAO56 crop water requirements method. Agric. Water Manag 243, 106466.
Pereira, L.S., Paredes, P., López-Urrea, R., Hunsaker, D.J., Mota, M., Mohammadi Shad, Z., 2021b. Standard single and basal crop coefficients for vegetable crops, an update of FAO56 crop water requirements approach. Agric. Water Manag 243, 106196.
Pereira, L.S., Paredes, P., Melton, F., Johnson, L., Wang, T., López-Urrea, R., Cancela, J. J., Allen, R.G., 2020. Prediction of crop coefficients from fraction of ground cover and height. Background and validation using ground and remote sensing data. Agric. Water Manag 241, 106197.
Pereira, L.S., Paredes, P., Oliveira, C.M., Montoya, F., López-Urrea, R., Salman, M., 2024. Single and basal crop coefficients for estimation of water use of tree and vine woody crops with consideration of fraction of ground cover, height, and training system for Mediterranean and warm temperate fruit and leaf crops. Irrig. Sci. 42, 1019–1058.
Petry, M.T., Magalhães, T.F., Paredes, P., Martins, J.D., Ferrazza, C.M., Hünemeier, G.A., Pereira, L.S., 2024. Water use and crop coefficients of soybean cultivars of diverse maturity groups and assessment of related water management strategies. Irrig. Sci. 42, 1–16.
Qin, S., Fan, Y., Li, S., Cheng, L., Zhang, L., Xi, H., Qiu, R., Liu, P., 2023. Partitioning of available energy in canopy and soil surface in croplands with different irrigation methods. Agric. Water Manag 288, 108475.
Qiu, R., Liu, C., Cui, N., Wu, Y., Wang, Z., Li, G., 2019. Evapotranspiration estimation using a modified Priestley-Taylor model in a rice-wheat rotation system. Agric. Water Manag. 224, 105755.
Ramos, T.B., Darouich, H., Oliveira, A.R., Farzamian, M., Monteiro, T., Castanheira, N., Paz, A., Gonçalves, M.C., Pereira, L.S., 2023. Water use and soil water balance of Mediterranean tree crops assessed with the SIMDualKc model in orchards of southern Portugal. Agric. Water Manag 279, 108209.
Reichstein, M., Falge, E., Baldocchi, D., Papale, D., Aubinet, M., Berbigier, P., Bernhofer, C., Buchmann, N., Gilmanov, T., Granier, A., Grunwald, T., Havrankova, K., Ilvesniemi, H., Janous, D., Knohl, A., Laurila, T., Lohila, A., Loustau, D., Matteucci, G., Meyers, T., Miglietta, F., Ourcival, J.-M., Pumpanen, J., Rambal, S., Rotenberg, E., Sanz, M., Tenhunen, J., Seufert, G., Vaccari, F., Vesala, T., Yakir, D., Valentini, R., 2005. On the separation of net ecosystem exchange into assimilation and ecosystem respiration: review and improved algorithm. Glob. Change Biol. 11, 1424–1439.
Rogers, J.S., Allen, L.H., Calvert, D.J., 1983. Evapotranspiration for humid regions: developing citrus grove, grass cover. Trans. ASAE 26 (6), 1778. -83, 92.
Segovia-Cardozo, D.A., Franco, L., Provenzano, G., 2022. Detecting crop water requirement indicators in irrigated agroecosystems from soil water content profiles: An application for a citrus orchard. Sci. Total Environ. 806, 150492.
Silva, R.M., Paço, T.A., Ferreira, M.I., Oliveira, M., 2008. Transpiration of a kiwifruit orchard estimated using the granier sap flow method calibrated under field conditions. Acta Hortic. (792), 593–600.
Taylor, N.J., Mahohoma, W., Vahrmeijer, J.T., Gush, M.B., Allen, R.G., Annandale, J.G., 2015. Crop coefficient approaches based on fixed estimates of leaf resistance are not appropriate for estimating water use of citrus. Irrig. Sci. 33, 153–166.
Wang, Y., Cai, H., Yu, L., Peng, X., Xu, J., Wang, X., 2020. Evapotranspiration partitioning and crop coefficient of maize in dry semi-humid climate regime. Agric. Water Manag 236, 106164.
Wang, Z., Chen, W., Piao, J., Cai, Q., Chen, S., Xue, X., Ma, T., 2025. Synergistic effects of high atmospheric and soil dryness on record-breaking decreases in vegetation productivity over Southwest China in 2023. Npj Clim. Atmos. Sci. 8, 6.
Wang, P., Li, S., Chen, Q., Li, X., Liu, S., Wu, X., Yang, X., Xu, Z., 2023. A novel method for simulating the dynamics of the single and dual maize crop coefficients in an arid ecosystem. Eur. J. Agron. 142, 126688.
Wiedemann, A., Marañón-Jiménez, S., Rebmann, C., Herbst, M., Cuntz, M., 2016. An empirical study of the wound effect on sap flux density measured with thermal dissipation probes. Tree Physiol. 36 (12), 1471–1484.
Williams, L.E., Ayars, J.E., 2005. Grapevine water use and the crop coefficient are linear functions of the shaded area measured beneath the canopy. Agric. For. Meteor. 132, 201–211.
Wilson, K., Goldstein, A., Falge, E., Aubinet, M., Baldocchi, D., Berbigier, P., Bernhofer, C., Ceulemans, R., Dolman, H., Field, C., Grelle, A., Ibrom, A., Law, B.E., Kowalski, A., Meyers, T., Moncrieff, J., Monson, R., Oechel, W., Tenhunen, J., Valentini, R., Verma, S., 2002. Energy balance closure at FLUXNET sites. Agric. For. Meteor. 113, 223–243.
Xiloyannis, C., Montanaro, G., Dichio, B., 2012. Kiwifruit In. Paper 66. In: Steduto, P., Hsiao, T.C., Fereres, E., Raes, D. (Eds.), Crop Yield Response to Water. FAO Irrig Drain, Rome, Italy, pp. 488–497. Paper 66.
Zhang, Y., Han, W., Zhang, H., Niu, X., Shao, G., 2023. Evaluating maize evapotranspiration using high-resolution UAV-based imagery and FAO-56 dual crop coefficient approach. Agric. Water Manag 275, 108004.
Zhang, B., Liu, Y., Xu, D., Zhao, N., Lei, B., Li, S., 2011. The evapotranspiration of a commercial apple orchard in the Loess Plateau, China. Agric. Water Manag 98 (4), 565–576.
Zhao, Y., Mao, X., Shukla, M.K., Tian, F., Hou, M., Zhang, T., Li, S., 2021. How does film mulching modify available energy, evapotranspiration, and crop coefficient during the seed-maize growing season in northwest China? Agric. Water Manag 245, 106666.